**Biogeosciences
Discussions**

High field NMR spectroscopy and FTICR mass spectrometry: powerful discovery tools for the molecular level characterization of marine dissolved organic matter from the South Atlantic Ocean

N. Hertkorn[1], M. Harir[1], B. P. Koch[2], B. Michalke[1], P. Grill[1], and
P. Schmitt-Kopplin[1]

[1]Research Unit Analytical Biogeochemistry, Helmholtz Zentrum München, Ingolstädter
Landstrasse 1, 85758 Neuherberg, Germany
[2]Alfred Wegener Institute, AWI, Am Handelshafen 12, 27570 Bremerhaven, (Building Co-5),
Germany

Correspondence to: N. Hertkorn (hertkorn@helmholtz-muenchen.de)

Title Page	
Abstract	Introduction
Conclusions	References
Tables	Figures
◄◄	►►
◄	►
Back	Close
Full Screen / Esc	
Printer-friendly Version	
Interactive Discussion	

Abstract

Non target high resolution organic structural spectroscopy of marine dissolved organic matter (DOM) isolated on 27 November 2008 by means of solid phase extraction (SPE) from four different depths in the South Atlantic Ocean off the Angola coast (3.1° E; −17.7° S; Angola basin) provided molecular level information of complex unknowns with unprecedented coverage and resolution. The sampling was intended to represent major characteristic oceanic regimes of general significance: 5 m (FISH; near surface photic zone), 48 m (FMAX; fluorescence maximum), 200 m (upper mesopelagic zone) and 5446 m (30 m above ground).

800 MHz proton (^{1}H) nuclear magnetic resonance (NMR) ^{1}H NMR, spectra were least affected by fast and differential transverse NMR relaxation and produced at first similar looking, rather smooth bulk NMR envelopes reflecting intrinsic averaging from massive signal overlap. Visibly resolved NMR signatures were most abundant in surface DOM but contributed at most a few percent to the total ^{1}H NMR integral and were mainly limited to unsaturated and singly oxygenated carbon chemical environments. The relative abundance and variance of resolved signatures between samples was maximal in the aromatic region; in particular, the aromatic resolved NMR signature of the deep ocean sample at 5446 m was considerably different from that of all other samples. When scaled to equal total NMR integral, ^{1}H NMR spectra of the four marine DOM samples revealed considerable variance in abundance for all major chemical environments across the entire range of chemical shift. Abundance of singly oxygenated CH units and acetate derivatives declined from surface to depth whereas aliphatics and carboxyl-rich alicyclic molecules (CRAM) derived molecules increased in abundance. Surface DOM contained a remarkably lesser abundance of methyl esters than all other marine DOM, likely a consequence of photodegradation from direct exposure to sunlight.

All DOM showed similar overall ^{13}C NMR resonance envelopes typical of an intricate mixture of natural organic matter with noticeable peaks of anomerics and C-aromatics

carbon whereas oxygenated aromatics and ketones were of too low abundance to result in noticeable humps at the S/N ratio provided. Integration according to major substructure regimes revealed continual increase of carboxylic acids and ketones from surface to deep marine DOM, reflecting a progressive oxygenation of marine DOM,
5 with concomitant decline of carbohydrate-related substructures.

Isolation of marine DOM by means of SPE likely discriminated against carbohydrates but produced materials with beneficial NMR relaxation properties: a substantial fraction of dissolved organic molecules present allowed the acquisition of two-dimensional NMR spectra with exceptional resolution. JRES, COSY and HMBC NMR spectra were
10 capable to depict resolved molecular signatures of compounds exceeding a certain minimum abundance. Here, JRES spectra suffered from limited resolution whereas HMBC spectra were constrained because of limited S/N ratio. Hence, COSY NMR spectra appeared best suited to depict organic complexity in marine DOM.

The intensity and number of COSY cross peaks was found maximal for sample
15 FMAX and conformed to about 1500 molecules recognizable in variable abundance. Surface DOM (FISH) produced a slightly (~25 %) lesser number of cross peaks with remarkable positional accordance to FMAX (~80 % conforming COSY cross peaks were found in FISH and FMAX). With increasing water depth, progressive attenuation of COSY cross peaks was caused by fast transverse NMR relaxation of yet unknown
20 origin. However, most of the faint COSY cross peak positions of deep water DOM conformed to those observed in the surface DOM, suggesting the presence of a numerous set of identical molecules throughout the entire ocean column even if the investigated water masses belonged to different oceanic regimes and currents.

Aliphatic chemical environments of methylene (CH_2) and methyl (CH_3) in marine
25 DOM were nicely discriminated in DEPT HSQC NMR spectra. Classical methyl groups terminating aliphatic chains represented only ~15 % of total methyl in all marine DOM investigated. Chemical shift anisotropy from carbonyl derivatives (i.e. most likely carboxylic acids) displaced aliphatic methyl ^{1}H NMR resonances up to δ_H ~1.6 ppm, indicative of alicyclic geometry which furnishes more numerous short range

High field NMR spectroscopy and FTICR mass spectrometry

N. Hertkorn et al.

Title Page

Abstract | Introduction

Conclusions | References

Tables | Figures

◄ | ►

◄ | ►

Back | Close

Full Screen / Esc

Printer-friendly Version

Interactive Discussion

connectivities for any given atom pairs. A noticeable fraction of methyl ($\sim 2\%$) was bound to olefinic carbon. The comparatively large abundance of methyl ethers in surface marine DOM contrasted with DOM of freshwater and soil origin. The chemical diversity of carbohydrates as indicated by H_2CO-groups ($\delta_C \sim 62 \pm 2$ ppm) and anomerics ($\delta_C \sim 102 \pm 7$ ppm) exceeded that of freshwater and soil DOM considerably.

HSQC NMR spectra were best suited to identify chemical environments of methin carbon (CH) and enabled discrimination of olefinic and aromatic cross peaks ($\delta_C > 110$ ppm) and those of doubly oxygenated carbon ($\delta_C < 110$ ppm). The abundance of olefinic protons exceeded that of aromatic protons; comparison of relative HSQC cross peak integrals indicated larger abundance of olefinic carbon than aromatic carbon in all marine DOM as well. A considerable fraction of olefins seemed isolated and likely sterically constrained as judged from small $^nJ_{HH}$ couplings associated with those olefins. High S/N ratio and fair resolution of TOCSY and HSQC cross peaks enabled unprecedented depiction of sp^2-hybridized carbon chemical environments in marine DOM with discrimination of isolated and conjugated olefins as well as α, β-unsaturated double bonds. However, contributions from five-membered heterocycles (furan, pyrrol and thiophene derivatives) even if very unlikely from given elemental C/N and C/S ratios and upfield proton NMR chemical shift ($\delta_H < 6.5$ ppm) could not yet been ruled out entirely. In addition to classical aromatic DOM, like benzene derivatives and phenols, six-membered nitrogen heterocycles were found prominent contributors to the downfield region of proton chemical shift ($\delta_H > 8$ ppm). Specifically, a rather confined HSQC cross peak at $\delta_H/\delta_C = 8.2/164$ ppm indicated a limited set of nitrogen heterocycles with several nitrogen atoms in analogy to RNA derivatives present in all four marine DOM. Appreciable amounts of extended HSQC and TOCSY cross peaks derived from various key polycyclic aromatic hydrocarbon substructures suggested the presence of previously proposed but NMR invisible thermogenic organic matter (TMOC) in marine DOM at all water depths. Eventually, olefinic unsaturation in marine DOM will be more directly traceable to ultimate biogenic precursors than aromatic unsaturation of which a substantial fraction originates from an aged material which from the beginning was

subjected to complex and less specific biogeochemical reactions like thermal decomposition.

The variance in molecular mass as indicated from Fourier transform ion cyclotron resonance (FTICR) mass spectra was limited and could not satisfactorily explain the observed disparity in NMR transverse relaxation of the four marine DOM samples. Likewise, the presence of metal ions in isolated marine DOM remained near constant or declined from surface to depth for important paramagnetic ions like Mn, Cr, Fe, Co, Ni and Cu. Iron in particular, a strong complexing paramagnetic ion, was found most abundant by a considerable margin in surface (FISH) marine DOM for which well resolved COSY cross peaks were observed. Hence, facile relationships between metal content of isolated DOM (which does not reflect authentic marine DOM metal content) and transverse NMR relaxation were not observed.

High field (12 T) negative electrospray ionization FTICR mass spectra showed at first view rather conforming mass spectra for all four DOM samples with abundant CHO, CHNO, CHOS and CHNOS molecular series with slightly increasing numbers of mass peaks from surface to bottom DOM and similar fractions ($\sim$50 %) of assigned molecular compositions throughout all DOM samples. The average mass increased from surface to bottom DOM by about 10 Dalton. The limited variance of FTICR mass spectra probably resulted from a rather inherent conformity of marine DOM at the mandatory level of intrinsic averaging provided by FTICR mass spectrometry, when many isomers unavoidably project on single nominal mass peaks. In addition, averaging from ion suppression added to the accordance observed. The proportion of CHO and CHNO molecular series increased from surface to depth whereas CHOS and especially CHNOS molecular series markedly declined. The abundance of certain aromatic CHOS compounds declined with water depth. For future studies, COSY NMR spectra appear best suited to assess organic molecular complexity of marine DOM and to define individual DOM molecules of yet unknown structure and function. Non-target organic structural spectroscopy at the level demonstrated here covered nearly all carbon present in marine DOM. The exhaustive characterization of complex unknowns

Full Screen / Esc

Printer-friendly Version

Interactive Discussion

in marine DOM will reveal a meaningful assessment of individual marine biogeosignatures which carry the holistic memory of the oceanic water masses (Koch et al., 2011).

1 Introduction

Marine dissolved organic matter (DOM) results from the combined action of biotic and abiotic reactions and physical distribution of water masses at different depths of the water column (Hansell and Carlson, 1998). It is one of the most abundant contributors to the global carbon and several other element cycles; nevertheless, marine DOM still ranges among the least characterized NOM fractions known (Dittmar and Kattner, 2003a; Hedges and Oades, 1997; Hernes and Benner, 2006). Local biochemical activity maxima in upwelling regimes, near deep sea vents or near large river plumes and processing of terrestrial precursor molecules in coastal areas (Dittmar and Kattner, 2003b; Hernes and Benner, 2006) contribute extensively to marine DOM biosynthesis; yet, our current knowledge and definition of its major contributors, like bacteria, archeae and viruses to marine DOM synthesis and decomposition remains poorly constrained (Jiao et al., 2010).

The recently proposed concept of the microbial carbon pump (MCP) (Jiao et al., 2010) supplements the classical view of marine carbon processing by the conventional biological pump. Here, regenerated production of organic matter by microbial heterotrophic activity is considered as a main source for accumulation of recalcitrant dissolved organic carbon. It is likely that both the conventional biological pump and the MCP operate in the turnover of marine organic matter. Significant primary production will occur in nutrient rich surface waters, whereas successive and perhaps repetitive processing of DOM by MCP will operate in a more diffuse manner throughout the entire ocean column. Vertical mixing (Hopkinson and Vallino, 2005), especially the downward transport of rather fresh particulate organic matter (POM) (Hedges et al., 2001) and DOM (Hopkinson and Vallino, 2005) meets with horizontal long-range transport of DOM with average ^{14}C ages of several millennia (Walker et al., 2011) and

imposes a complex distribution pattern of DOM production and degradation reactions (Hansell and Carlson, 1998). Prominent abiotic reactions like photochemistry (Schmitt-Kopplin et al., 1998; Zepp et al., 2011) and atmospheric deposition (both strongest near the surface) (Andreae and Crutzen, 1997; Jimenez et al., 2009; Paytan et al., 2009), (metal-mediated) redox chemistry (Schmidt et al., 2011), and thermogenic process-ing of organic matter (Dittmar and Koch, 2006; Dittmar and Paeng, 2009; Falco et al., 2011) continually attenuate and diminish the biological signatures of marine DOM which ultimately arise from primary production.

Degradative DOM analysis has revealed carbohydrates, amino acids and lipids as key biological constituents of marine DOM (Benner, 2002); at increasing water depth, the proportion of assigned carbon covered by these classes of molecules progressively diminishes from 20 % to less than 2 % of total carbon (Benner, 2002). Recently, thermo-genic organic carbon (TMOC) of considerable ^{14}C age (on average, several ten thou-sands of years) which shows abundance in hydrogen-deficient aromatic molecules, has been detected in appreciable amounts (a few percent of total DOM) throughout the oceans, comparable in abundance to the three major classes of biological molecules (Dittmar and Koch, 2006; Dittmar and Paeng, 2009). TMOC may originate from deep sea vents or other oceanic underground sources (Dittmar and Koch, 2006) and from riverine transport (Battin et al., 2009) of terrestrial black carbon into the ocean (Falco et al., 2011). TMOC passively correlates with salinity, suggesting photodegradation in the surface ocean as a plausible degradation mechanism (Dittmar and Paeng, 2009).

Non-target organic structural spectroscopy of DOM attempts to unselectively charac-terize the entire carbon present in DOM by means of information-rich detection meth-ods such as Fourier transform ion cyclotron resonance (FTICR) mass spectrometry and NMR spectroscopy (Einsiedl et al., 2007; Hertkorn et al., 2006, 2008, 2007; Mop-per et al., 2007; Schmitt-Kopplin et al., 2010a, b). FTICR mass spectrometry of DOM allows for an unprecedented resolution of thousands of molecular formulae direct out of the DOM mixture, however with considerable selectivity depending on sample handling and ionization method applied (Hertkorn et al., 2008; Koch et al., 2005; Kujawinski,

2002; Stenson et al., 2003; Flerus et al., 2011b; Kujawinski et al., 2009). NMR on the other hand allows for a successive acquisition of multiple informative complementary NMR spectra at however lesser sensitivity (Simpson et al., 2002, 2011; Hertkorn and Kettrup, 2005). One-dimensional NMR spectra provide near quantitative data when carefully acquired. While acquisition of NMR spectra at high magnetic field strength (B_0) is desirable because of excellent resolution and intrinsic sensitivity and dispersion gain, transverse relaxation (loss of coherence and entropy gain because of atomic motion) may become faster at larger B_0 (Kleckner and Foster, 2011). Higher dimensional NMR spectra of complex organic mixtures of polar and ionisable molecules like those present in marine DOM may show convoluted signatures of chemical composition and physical interactions which could attenuate cross peak integral at high resolution if magnetization is lost with fast relaxation.

Molecular level NOM composition and structure often exhibit far more variance than anticipated from often rather uniform bulk parameters which are subject to intrinsic averaging (Ritchie and Perdue, 2008; Kelleher and Simpson, 2006; Mahieu et al., 1999; Hertkorn et al., 2007). This study aims to use high field NMR spectroscopy ($B_0 = 18.8$ T, corresponding to 800 MHz ^{1}H NMR frequency, with cryogenic detection) and FTICR mass spectrometry ($B_0 = 12$ T) as non-target discovery tools to resolve characteristic molecular signatures of a specific, representative set of four selected marine DOM samples obtained by solid phase extraction (SPE). These four DOM samples were collected during an extensive SPE mapping study of marine waters across the East Atlantic Ocean during the R/V *Polarstern* cruise ANT XXV/1 and shared the common extraction material used (PPL, a styrene divinyl copolymer), the position of sampling (3.1° E; −17.7° S) and the water sampling depth used was 5 m (near surface photic zone), 48 m (fluorescence maximum), 200 m (upper mesopelagic zone) and 5446 m (30 m above ground) to represent major characteristic oceanic regimes of global relevance.

2 Methods

2.1 Sampling area and DOM extraction

Atlantic Ocean water samples were collected during the R/V *Polarstern* cruise ANT XXV/1 on 27 November 2008 at $3.126°$ E, $-17.737°$ S by means of a Teflon lined, towed fish sampler and CTD cast, as described in Koch and Kattner (2011). Immediately after sampling, the water (50 l aliquots) was filtered (Whatman GF/F glass fiber; precombusted at 450 °C) and subjected to solid phase extraction by means of PPL, a styrene divinyl copolymer which is tailored for the retention of highly polar to non-polar substances from large volumes of water (Dittmar et al., 2008; Kaiser et al., 2003). Water was acidified (pH 2) with 10 M HCl and gravitationally rinsed through 6 g PPL solid-phase extraction cartridges (PPL, Varian Bond Elut; Table 1) (Dittmar et al., 2008; Kaiser et al., 2003). Finally, the DOM was eluted with about 50 ml of pure methanol (Merck, Darmstadt, Germany). The eluted samples were stored at -27 °C in the dark until use. For NMR spectroscopy, aliquots of original CH_3OH solutions of marine DOM samples were evaporated in vacuo to dryness and CD_3OD was added; this cycle was repeated three times to largely exchange methanol-h_4 by methanol-d_4. Here, yellow, somewhat grainy solid marine DOM was obtained, sometimes accompanied by tiny amounts of white materials evenly distributed in the flask at the level of initial liquid phase.

2.2 NMR analysis

All proton detected NMR spectra were acquired immediately after sample preparation with a Bruker Avance III NMR spectrometer operating at 800.13 MHz ($B_0 = 18.8$ T) and TopSpin 3.0/PL3 software with samples from redissolved solids (9–36 mg solid DOM in typically 120–225 µl CD_3OD (99.95 % ^2H), Aldrich, Steinheim, Germany; Table 1) in sealed 2.5 and 3.0 mm Bruker Match tubes. Proton spectra were acquired with an inverse geometry 5 mm z-gradient $^1H/^{13}C/^{15}N/^{31}P$ QCI cryogenic probe (90°

excitation pulses: $^{13}C \sim {}^{1}H \sim 10\,\mu s$) whereas carbon detected NMR spectra were also acquired with a 3 mm z-gradient QCO $^{13}C(^{15}N,^{31}P)/^{1}H$ cryogenic probe (90° excitation pulses: $^{13}C \sim 5.3\,\mu s$ and $^{1}H \sim 17\,\mu s$). NMR shift reference: ^{1}H NMR, HD_2OD: 3.30 ppm, DMSO-d_6: 2.49 ppm; ^{13}C NMR, CD_3OD: 49.00 ppm. All spectra were ac-
5 quired at 283 K to impede side reactions during NMR acquisitions. Comparison of ^{1}H NMR spectra acquired before and after lengthy acquisitions showed negligible alterations (Flerus et al., 2011b). 1-D ^{1}H NMR spectra were recorded with a spin-echo sequence (10 μs delay) to allow for high-Q probe ringdown; classical presaturation "*zgpr*" and "*zgpurge*" (Simpson and Brown, 2005) and solvent suppression with presatura-
10 tion and 1 ms spin-lock (*noesygppp1d*), 5 s acquisition time, 15 s relaxation delay d1, typically 512 scans, 1 Hz exponential line broadening were applied. Another set of ^{1}H NMR spectra of marine DOM was acquired in dry DMSO-d_6 under exclusion of moisture (Kovalevskii et al., 2000; Hertkorn et al., 2006) in sealed 5 mm tubes from 500 μg of DOM in 750 μl DMSO-d_6 (99.95 % ^{2}H, Aldrich, Steinheim, Germany) at $B_0 = 18.8$ T
15 and 11.7 T; an acquisition time of 5 s and a relaxation delay of 5 s was used with a spin echo sequence (10 μs delay time). ^{13}C NMR spectra used inverse gated WALTZ-16 decoupling (19 s relaxation delay; typically 10 000–35 000 scans) with an acquisition time (aq) of 1 s and an exponential line broadening of 12.5 Hz. Methanol-d_4 NMR resonances could be fitted with Lorentzian lineshapes in the chemical shift range from
20 $\delta_C \sim 48 \ldots 49.5$ ppm and subtracted from the ^{13}C NMR spectra (data not shown). However, excellent lineshape and high magnetic field made this a cosmetic exercise for interest rather than a mandatory visual improvement. ^{13}C DEPT NMR spectra were acquired with aq = 1 s and d1 = 2 s; the one bond coupling constant $^{1}J(CH)$ used in 1-D ^{13}C DEPT and 2-D $^{1}H,^{13}C$ DEPT-HSQC spectra was set to 145 Hz and 135 Hz
25 (the latter for CH_2 and CH_3 subspectra). DEPT-HSQC spectra were acquired with 16 scans and 1024 increments with a carbon sweep width of 40 kHz (200 ppm). Individual ^{1}H and multiplicity-edited ^{13}C NMR traces obtained from linear combinations of DEPT NMR spectra were integrated with a bucket width of 0.01/1 ppm (AMIX software, version 3.9.4) to produce the ^{1}H NMR overlay spectra (Fig. 3, Supporting Online

Fig. 2) and the NMR section integrals provided in Tables 3 and 4. Carbon decoupled ^{1}H, ^{13}C HSQC spectra (*hsqcetgpsisp2.2*) were acquired under the following conditions: acquisition time: 250 ms; ^{13}C 90° decoupling pulse, GARP (70 µs); 50 kHz WURST 180° ^{13}C inversion pulse (**W**ideband, **U**niform, **R**ate, and **S**mooth **T**runcation; 1.2 ms); F2 (^{1}H): spectral width of 9615 Hz, ^{1}J(CH) = 150 Hz, 1.25 s relaxation delay; F1 (^{13}C): SW = 40 253 Hz (200 ppm); number of scans (F2)/F1-increments (^{13}C frequency) for DOM (400–1800/137–142). HSQC-TOCSY (*hsqcetgpsisp.2*) NMR spectra used dipsi-2 mixing of 70 ms. Non-decoupled absolute value accordion (^{1}J$_{CH}$ = 135–165 Hz; ^{n}J$_{CH}$ = 5–10 Hz) HMBC spectra (*hmbcacbigplnd*) were acquired with aq = 400 ms and d1 = 1.1 s. All HSQC-derived NMR spectra were computed to a 8192 × 1024 matrix (HMBC: 16384 × 512) with exponential line broadening of 3 Hz in F2 (DOM) and a shifted sine bell ($\pi/2.5$) in F1. Gradient (1 ms length, 200 µs recovery) and sensitivity enhanced sequences were used for all HSQC, DEPT-HSQC and TOCSY NMR spectra. COSY and TOCSY NMR spectra used acquisition times of 750 ms at a spectral width of 9615 Hz with 70 ms dipsi-2 mixing sequence (TOCSY with solvent suppression: *dipsi2etgpsi19*), and absolute value (COSY) and echo-antiecho selection (TOCSY) with variable relaxation delay d1, ranging from 750 ms to 3.25 s, depending on T_1 noise attenuation and induced temperature variance; 16 scans/1600 increments were acquired. COSY/TOCSY spectra were computed to a 8192 × 2048 matrix with 2.5 Hz exponential multiplication in F2 and a shifted sine bell ($\pi/2.5$; TOCSY) and squared shifted sine bell ($\pi/2.5$; COSY) in F1.

NMR chemical shifts and NMR spectra for the proposed model of substituted polycyclic aromatics (Fig. 12, Supporting Online Fig. 5 and Supporting Online Table 2) were computed from ACD HNMR and CNMR predictor software, version 5.0 (Advanced Chemistry Development, Toronto, Canada). Further NMR acquisition parameters are provided in the Supporting Online Table 1; see also Table 1.

2.3 FTICR mass spectrometry

Ultrahigh-resolution Fourier transform ion cyclotron (FTICR) mass spectra were acquired using a 12 T Bruker Solarix mass spectrometer (Bruker Daltonics, Bremen, Germany) and an electrospray ionization source in negative mode. Diluted marine DOM ($5\,\mu g\,ml^{-1}$ in methanol) were injected into the electrospray source using a microliter pump at a flow rate of $120\,\mu l\,h^{-1}$ with a nebulizer gas pressure of 138 kPa and a drying gas pressure of 103 kPa. A source heater temperature of 200 °C was maintained to ensure rapid desolvatation in the ionized droplets. Spectra were first externally calibrated on clusters of arginine in MeOH ($0.57\,\mu mol\,l^{-1}$) and internal calibration was systematically done in the presence of natural organic matter reaching accuracy values lower than 500 ppb. The spectra were acquired with a time domain of 4 megawords and 1000 scans were accumulated for each spectrum. Calculation of elemental formulas for each peak was done in a batch mode by an in-house written software tool. The generated formulae were validated by setting sensible chemical constraints [N rule, O/C ratio ≤ 1, H/C ratio $\leq 2n + 2$ (C_nH_{2n+2}), element counts: $C \leq 100$, $H \leq 200$, $O \leq 80$, $N \leq 3$, $S \leq 2$, $P \leq 1$ and mass accuracy window (set at ± 0.5 ppm)]. Final formulae were generated and categorized into groups containing CHO, CHNO, CHOS or CHNOS molecular compositions which were used to reconstruct the group-selective mass spectra (Schmitt-Kopplin et al., 2010). The computed average values for H, C, N, O and S (atom %) and the H/C and O/C ratios given in Table 5 were based upon intensity-weighted averages of mass peaks with assigned molecular formulae.

2.4 Metal analysis of methanolic DOM extract

From each original methanolic DOM extract exactly weighted (range 40–50 mg) solutions were gently evaporated using a "Digiprep-system" (S-Prep, Germany), and the residuals were re-dissolved with very pure 30 m 1 % HNO_3. These solutions were used for analysis with ICP-AES (inductive coupled plasma atom emission spectroscopy; Optima 7300, Perkin Elmer, Rodgau-Jügesheim, Germany) or, in case when

High field NMR spectroscopy and FTICR mass spectrometry

N. Hertkorn et al.

Title Page

Abstract | Introduction

Conclusions | References

Tables | Figures

Back | Close

Full Screen / Esc

Printer-friendly Version

Interactive Discussion

concentrations were found below the instrument limit of detection (LoD), with a high resolution ICP-sf-MS (inductive coupled plasma sector field mass spectrometer; Element-1, Thermo-Finnigan, Bremen). Instrument Parameters for ICP-AES (inductive coupled plasma atom emission spectroscopy): the RF power was 1000 W, the plasma gas was 15 l Ar/min, and the nebuliser gas was 0.6 l Ar/min. A Micromist nebulizer was connected to a cyclon spray chamber. The measured spectral element lines were (nm): Al: 396.153, As: 193.696, B: 249.772, Ca: 393.366, Cu: 324.752, Fe: 259.939, K: 766.490, Mn: 257.610, Mo: 202.031, Na: 589.592, Ni: 231.604, P: 213.617, S: 181.975, Zn: 213.857.

High resolution ICP-sf-MS (inductive coupled plasma sector field mass spectrometry): Sample introduction was carried out using a peristaltic pump equipped with an "anti-pulse-head" (SPETEC, Erding, Germany), connected to a Micromist nebulizer with a cyclon spray chamber. The RF power was 1200 W, the plasma gas was 15 l Ar/min, and the nebuliser gas was 0.9 l Ar/min. The measured isotopes were: ^{9}Be, ^{209}Bi, ^{114}Cd, ^{59}Co, ^{52}Cr, ^{133}Cs, ^{202}Hg, ^{7}Li, ^{24}Mg, ^{55}Mn, ^{58}Ni, ^{208}Pb, ^{121}Sb, ^{120}Sn, ^{88}Sr, ^{232}Th, ^{48}Ti, ^{238}U.

Quality control was performed for ICP-AES and ICP-sf-MS: Before and after sample measurements control determinations of blanks and certified standards for all mentioned elements were performed. Calculation of results was carried out on a computerized lab-data management system, relating the sample measurements to calibration curves, blank determinations, control standards and the weight of the digested samples.

3 Results and discussion

3.1 Details of solid phase extraction of marine DOM from seawater

A large volume of seawater (~50 l each) was processed to eventually obtain NMR spectra with a good S/N ratio; hence, the amount of isolated marine DOM at last

outbalanced conceivable organic impurities possibly originating from the SPE cartridge itself. SPE extraction discriminated against DON, especially at deep waters; the C/N ratio for all extracts ranged near 25 (Table 1), placing credible restraints on the maximum occurrence of peptides in isolated marine DOM.

The water masses covered by our sampling represent Atlantic surface water (5 m, 48 m, 200 m) and North Atlantic Deep Water (NADW, 5446 m). The depth profile (Fig. 1) was characterized by the typical decreasing DOC/DON concentration induced by primary production in the surface whereas older water masses (North Atlantic Deep Water, NADW, Fig. 1) carried predominantly refractory DOM in the deeper layers (for details, see Koch et al., 2011).

3.2 Intrinsic aspects of high-field NMR spectroscopy related to sensitivity and resolution in complex mixtures

Solution NMR spectroscopy at 800 MHz ($B_0 = 18.8$ T) with cryogenic detection offers ultimate sensitivity and dispersion (Kovacs et al., 2005). Both items are very useful for analysis of marine NOM, an extremely intricate organic mixture, which occurs at low concentrations (<1 mg l^{-1} seawater) and shows low-resolution signatures in one-dimensional proton and carbon NMR spectra because of prevalent superposition of many NMR resonances at any data point (Hertkorn et al., 2007). Notably, individual NMR experiments carry specific intrinsic nominal resolution. Here, two-dimensional NMR spectra not only exceed the nominal resolution of 1-D NMR spectra considerably (Table 2), but 2-D NMR pulse sequences also act as filters to selectively emphasize individual transfers of magnetization such as certain homonuclear and heteronuclear spin-spin couplings (Cavanagh et al., 2007; Hertkorn et al., 2002b). Hence, 2-D NMR spectra of NOM commonly exhibit a vastly superior effective resolution even if they might represent a lesser overall number of NMR resonances than those which define a 1-D NMR spectrum. Analogously, individual NMR experiments will carry intrinsic characteristics with respect to spectral resolution or/and S/N ratio which can be selectively pronounced and attenuated by judicious choice of acquisition and apodization

parameters (Hoch and Stern, 1996).

Increased NMR detection sensitivity at high magnetic field B_0 might elevate potential interferences intrinsic to NMR to the level of observation which otherwise would be lost in noise. NMR spectra represent operating quantum mechanics with macroscopic observables, which carry information about chemical environments of atoms as well as of physical phenomena, like atomic and molecular mobility (Carper et al., 2004; Case, 1998; Cook et al., 1996; Effemey et al., 2000; Ying et al., 2006). The different NMR experiments will react unequal to these challenges. For example, NMR experiments with long intrinsic duration and variable magnetization transfer/relaxation delays (like 2-D NMR experiments) will be more susceptible to effects of fast and differential relaxation than rather short duration NMR pulse sequences (like 1-D NMR experiments).

The Larmor equation of NMR [$\omega_i = \gamma_N \, B_0 \, (1 - \delta_i)$; γ_N = gyromagnetic ratio] implies that actual NMR frequencies ω_i are proportional to the external magnetic field B_0. Likewise, NMR total chemical shift ranges as well as frequency differences $\Delta\omega_{ij}$ between dissimilar chemical environments ω_i and ω_j scale with B_0. Nevertheless, NMR spectra are visualized as plots of line intensity versus frequency ω_i, expressed as dimensionless, magnetic field independent units of chemical shift δ_i. Hence, the effects of differential NMR relaxation which itself depend on atomic and molecular mobility on frequency timescales (Korzhnev et al., 2004a; Neudecker et al., 2009) are magnetic field dependent and proportional to B_0^m ($m \geq 1$, depending on the actual relaxation mechanism; Bakhmutov, 2004).

NMR relaxation strongly affects NMR spectra: fast transverse relaxation directly relates to line broadening in one and two-dimensional NMR spectra (Cavanagh et al., 2007). In the latter, fast transverse relaxation will attenuate cross peak intensities at higher F1 increments, resulting in lesser overall S/N ratio at long acquisition times and often noticeable diminished F1 resolution. Two major molecular mechanisms induce fast transverse NMR relaxation: larger molecules exhibit higher proportions of low frequency atomic and molecular motions which impose efficient transverse relaxation (Hansen and Al-Hashimi, 2007; Korzhnev et al., 2004b). In case of DOM, effects of

Title Page

Abstract | Introduction

Conclusions | References

Tables | Figures

◄ | ►

◄ | ►

Back | Close

Full Screen / Esc

Printer-friendly Version

Interactive Discussion

differential transverse NMR relaxation, which might lead to significant line broadening are rather expected for molecular units of low mobility and low local symmetry (e.g. sp^2-hybridized carbon) (Buddrus et al., 1989). All sp^2-hybridized carbon chemical environments in marine DOM will be subject to fast NMR relaxation at high magnetic field (here: $B_0 = 18.8$ T) because of a significant contribution of chemical shift anisotropy (CSA) to transverse relaxation (Hansen and Al-Hashimi, 2007; Carper et al., 2004; Korzhnev et al., 2004b; Effemey et al., 2000; Mulder and Akke, 2003). Therefore, marine DOM NMR resonances derived from sp^2-hybridized carbon (commonly $\delta_C > 110$ ppm) are expected to suffer more from (HSQC and HMBC) cross peak attenuation at higher F1 increments in 2-D NMR spectra than other NMR resonances derived from sp^3-hybridized carbon (commonly $\delta_C < 110$ ppm). Another, fundamentally different mechanism for enhanced longitudinal and transverse NMR relaxation is caused by free electrons in radicals and (paramagnetic) metal ions (Smernik and Oades, 1999, 2000, 2002). Metal ions in marine waters might coordinate several DOM ligand molecules (Witter et al., 2000; Pohl et al., 2011; Vraspir and Butler, 2009; Hertkorn et al., 2004) and therefore reduce their apparent mobility. In addition, coordination compounds of marine DOM with paramagnetic 3d metal ions like V, Mn, Cr, Fe, Co, Ni, and Cu will be plausible candidates for fast relaxing species of low NMR visibility (Bertini et al., 2008).

COSY and JRES NMR spectra are commonly computed with strongly truncating apodization functions which are designed to emphasize cross peak resolution and good pattern depiction. This behaviour will discriminate in favour of molecules which exceed a certain minimum abundance, a typical feature expected for common biological and abundant biogeochemical signatures. JRES NMR spectra offer rarely any liberty in selecting apodization functions beyond unshifted sine-bells in absolute value modus to accommodate for complex cross peak amplitudes from remote $^nJ_{HH}$ couplings and limited nominal NMR matrix size (Table 2). COSY NMR spectra with a $\sim$300 times larger nominal matrix size than available in JRES NMR spectra offer improved depiction of NOM organic complexity and liberty to employ mixed apodization functions to selectively enhance either cross peak resolution or S/N ratio. However, the antiphase

character of COSY cross peaks will make them susceptible to attenuation and possibly self-cancellation in case of larger linewidths as a consequence of fast transverse NMR relaxation. TOCSY NMR spectra offer absorptive lineshape cross peaks which are best suited for sensitive detection of minor NOM signatures, e.g. in the aromatic region, and offer $1/2 \times {}^{n}J_{HH}$ transfer time as opposed to $1/{}^{n}J_{HH}$ in COSY NMR spectra (Hertkorn et al., 2002b).

One-dimensional NMR spectra are commonly apodized to enhance S/N ratio by easily adjustable exponential multiplication which leaves spectral line area ratios invariant but not amplitude ratios. Hence, the matched filter concept (Traficante and Rajabzadeh, 2000; Spencer, 2010) is not unambiguously defined in marine DOM because of variable linewidth. The dramatic effects of educated apodization (Hertkorn et al., 2002a; Hoch and Stern, 1996) are demonstrated in Fig. 2 in which a TOCSY NMR spectrum of DOM sample FMAX is computed with an apodization designed to enhance S/N ratio at the expense of resolution (Fig. 2, panels 1A, 1B), whereas apodization optimized for resolution enhancement is applied in panels (1C) and (1D), respectively. Faint and rather expansive TOCSY cross peaks ($\delta_H \sim 5 \ldots 10$ ppm) became visible at large S/N ratio (Fig. 2, panel 1A) which were not at all discernible in case of resolution enhancement used (panel 1C). Instead, resolution enhancement brought out sharp resolved cross peak patterns indicative of small, and relatively abundant molecules which otherwise were lost in expansive low-resolution cross peaks with minimal recognizable features.

3.3 ^{1}H NMR spectra of marine DOM

The ^{1}H NMR spectra of the four DOM samples acquired with and without (data not shown) solvent suppression showed the smooth bulk envelopes familiar from other marine DOM spectra (Fig. 3) (Aluwihare et al., 2002; Hertkorn et al., 2006; Repeta et al., 2002). From higher to lower field (from right to left), abundant (a) aliphatics, (b) "acetate-analogue", (c) carboxyl-rich alicyclic molecules CRAM, (d) "carbohydrate-like" and methoxy, (e) olefinic, and (f) aromatic NMR resonances showed well visible

and rather broad maxima (letters given according to Supporting Online Fig. 2). Superimposed small NMR resonances indicative of comparatively abundant biological and biogeochemical molecules were most significant in the aromatic section (f), well noticeable in sections (d) and (e) and of continual lesser occurrence in the order c > b > a.

In general, the abundance of proton NMR recognizable molecular signatures declined in the order FMAX > FISH >> 200 m > 5446 m; i.e. it correlated with the supposed biological activity and primary production in the photic zone. With the bulk envelopes dominating the NMR spectra, the relative intensity distributions nevertheless showed appreciable variation which appeared more conspicuous in the spectral overlay (Fig. 3A–D) than in the relative NMR section integrals (Table 3, Supporting Online Fig. 1). In fact, given the extent of mandatory intrinsic averaging in proton 1-D NMR spectra, the observed variance across the ^{1}H NMR spectra of the four marine DOM samples has to be appraised as very relevant (Fig. 3D).

The proton NMR spectra of four marine DOM shown (Fig. 3; Supporting Online Fig. 2) were normalized to identical areas of total integral from $\delta_H \sim 0\ldots10.5$ ppm. The signal envelopes showed smooth overall distribution with nearly coinciding methyl resonances near $\delta_H \sim 0.9$ ppm (methyl, terminating purely aliphatic chains), variable intensity maxima at $\delta_H \sim 1.3$ ppm (methylene and other purely aliphatics, $\underline{H}C \geq 4$ bonds away from next heteroatom) and progressively increasing downfield shoulders ranging from $\delta_H \sim 1.4\ldots1.7$ ppm in the order FISH < FMAX < 200 m < 5446 m, which represented mostly alicyclic rings with a large proportion of methyl groups (cf. DEPT HSQC spectra; Figs. 8, 9). The abundance of acetate derivatives near $\delta_H \sim 2.1$ ppm declined from surface to deep DOM, whereas functionalized aliphatics including those with remote carboxylic substitution typical of carboxyl-rich alicyclic molecules (CRAM; heteroatoms ≥ 2 bonds away from protons; $\delta_H \sim 2.2\ldots3.2$ ppm) showed the opposite trend. The sum of purely aliphatic (heteroatoms ≥ 4 bonds away $\delta_H \sim 0\ldots1.9$ ppm) and functionalized (heteroatoms ≥ 3 bonds away; $\delta_H \sim 1.9\ldots3.1$ ppm) protons increased from surface to bottom DOM, however slightly. Singly oxygenated units ($\underline{H}C$-O) divided in methoxy derivatives ($\delta_H \sim 3.6\ldots3.8$ ppm), carbohydrates, esters and others

High field NMR spectroscopy and FTICR mass spectrometry

N. Hertkorn et al.

Title Page

Abstract	Introduction
Conclusions	References
Tables	Figures

◄ | ►

◄ | ►

Back | Close

Full Screen / Esc

Printer-friendly Version

Interactive Discussion

($\delta_H \sim 3.4\ldots 4.8$ ppm). When scaled to the total integral across the entire chemical shift range, methoxy derivatives showed maximum occurrence at sample FMAX and otherwise declined from surface to bottom, whereas general oxygenated units declined from surface to bottom DOM (Fig. 3, Table 3). When normalized to 100 % abundance within the <u>H</u>C-O chemical shift section from $\delta_H \sim 3.4\ldots 4.8$ ppm (Fig. 3D), methoxy peaks declined in the order FMAX > 200 $\sim$ 5446 > FISH. Here, classical carbohydrates ($\delta_H \sim 3.4\ldots 4.1$ ppm) appeared most abundant for surface sample FISH (Fig. 3d).

Variable proportions of olefins ($\delta_H \sim 5\ldots 7$ ppm) and aromatics ($\delta_H \sim 7\ldots 10$ ppm) contributed to unsaturated chemical environments of protons. The combined abundance of protons bound to sp^2-hybridized carbon (i.e. olefins and aromatics) decreased from surface to 200 m and slightly increased near the ocean bottom. A group of NMR resonances with small J_{HH} couplings ($^n J_{HH} < 3$ Hz; cf. JRES and COSY NMR spectra) at $\delta_H \sim 6.4$ ppm (Fig. 3B; cf. also Supporting Online Fig. 1, Supporting Online Fig. 2) with declining abundance from surface to deep marine DOM (Korzhnev et al., 2004b; McCaul et al., 2011), recognized earlier in ultrafiltered marine NOM (Hertkorn et al., 2006) and lake sediments (data not shown) but not previously assigned can now be attributed to (remotely substituted) olefins by means of HSQC cross peaks (near $\delta_C \sim 110$ ppm). Analogous isolated double bonds can be found in linear terpenoids and double bonds within aliyclic systems, suggesting (in line with its declining distribution pattern from surface to depth) biological origin of these olefins. The olefinic NMR envelopes of surface samples FISH and FMAX on the one hand and of the deep samples 200 m and 5446 m on the other hand nearly coincided (Fig. 3B) and the olefinic/aromatic proton NMR integral ratio varied from 1.78 (FISH), 1.89 (FMAX), 2.11 (200 m) to 1.41 (5446 m; Table 3). Hence, the abundance of olefinic protons in marine DOM always exceeded that of aromatic protons. The aromatic section (f; Supporting Online Fig. 2) showed the largest proportion of recognizable NMR signatures, the most extensive variation in NMR resonance distribution and therefore the most pronounced distinct own signature (cf. also COSY NMR spectra). Here, the deep sea aromatic protons differed most from all other groups and suggested the presence of

High field NMR spectroscopy and FTICR mass spectrometry

N. Hertkorn et al.

an unique deep sea molecular signature which could have resulted from long term DOM processing and, alternatively, DOM leaching from bottom sediments across the expansive seafloor.

NMR resonances indicative of $\underline{H}$C-O environments ($\delta_H \sim 3.1\ldots4.9$ ppm) occurred in the order FMAX > FISH > 200 m > 5446 m and commonly showed an intensity maximum near $\delta_H \sim 3.65$ ppm, probably caused by methoxy groups ($\delta_H \sim 3.6\ldots3.8$ ppm; cf. discussion of JRES, TOCSY and (DEPT) HSQC NMR spectra). However, the relative intensity distributions within this group of NMR resonances changed considerably (Fig. 3D): the deep DOM (5446 m) exhibited a noticeable downfield shoulder which progressively developed from FMAX to bottom DOM (cf. assignment in DEPT HSQC NMR spectra). Both surface (FISH and FMAX) samples showed abundant resolved $\underline{H}$C-O NMR resonances with almost identical distribution in the chemical shift range from $\delta_H \sim 3.35\ldots4.7$ ppm with however much more prevalent OCH$_3$-derived NMR resonances (from $\delta_H \sim 3.6\ldots3.8$ ppm) present in sample FMAX. Both deep DOM samples (200 m and 5446 m) showed rather smooth and nearly coinciding NMR envelopes from $\delta_H \sim 3.35\ldots4.1$ ppm with abundant methylester peaks at $\delta_H \sim 3.6\ldots3.8$ ppm; in case of the 5446 m sample, possibly a few aromatic methyl esters ($\delta_H > 3.75$ ppm) appeared with a more distinct shoulder. After scaling the ^{1}H NMR spectra of the two surface and deep DOM samples to maximum accordance across the entire $\underline{H}$C-O chemical shift range (Fig. 3D), the intensity maxima for DOM samples were in the order FMAX > 5446 m ~ 200 m > FISH with surface sample FISH strongly (by >20 %) attenuated. The lesser abundance of methyl esters in surface DOM FISH sample (cf. DEPT HSQC NMR spectra) could be plausibly explained by selective photodegradation from strong exposure to direct sunlight (Zepp et al., 2011; Schmitt-Kopplin et al., 1998).

3.4 ^{13}C NMR spectra of marine DOM

Surprisingly, ^{13}C NMR spectra of our marine DOM samples could not readily be acquired with acceptable baseline with an inverse 5mm QCI probehead (optimized for ^{1}H NMR sensitivity with an outer ^{13}C and an inner ^{1}H coil) in which the 90° ^{13}C excitation

hard pulse ranged near 10 µs at $B_0 = 18.8$ T (carbon frequency: 201.26 MHz). This applied to a range of experimental conditions, including single pulse excitation and spin-echo sequences (Buddrus et al., 1989) with 10 µs delay and various adiabatic refocusing pulses (up to 70 kHz bandwidth) (Xia et al., 2008). The available composite 180° refocusing pulses with a duration of several µs to diminish effects of fast transverse NMR relaxation exhibited limited excitation bandwidth (Martin et al., 2010) which so far were not sufficient to evenly excite the full range of the ^{13}C NMR spectrum (here: 235 ppm, analogous to 47 kHz). This behaviour appeared specific to these marine DOM samples because mixtures of small molecules in a repertory of organic solvents including CD_3OD could be readily detected with the same NMR experimental setup. Several delay periods from 8 µs to 40 µs were employed in single pulse sequences between pulse and first acquisition data point to account for ringdown which takes longer time for high-Q NMR probeheads. However, acceptable baseline could again not be reached, also with use of backward linear prediction (data not shown). Marine DOM harbours arrays of superimposed narrow and broad NMR resonances because of extensive intricacy which do not reach the baseline across nearly the entire chemical shift range in ^{1}H and ^{13}C NMR spectra. The Avance III NMR console offers options for digital signal enhancements (Moskau, 2002) to likely overcome these problems in future; these are, however, beyond the scope of this publication.

Fortunately, meaningful ^{13}C NMR spectra of the four marine DOM samples at $B_0 = 18.8$ T (carbon frequency: 201.26 MHz) with acceptable baseline could be acquired with a 3 mm QCO probehead with classical geometry [optimized for observation of heteronuclei with an inner X (^{13}C, ^{15}N, ^{31}P) and an outer ^{1}H coil] with a 90° ^{13}C excitation hard pulse of 5.3 µs, allowing for a sufficient excitation bandwidth with a spin echo sequence using 10 µs delay (Fig. 4) and a composite refocusing 180° pulse.

Initially, the individual ^{13}C DEPT-45, -90 and -135 NMR spectra of all four marine DOM (Buddrus et al., 1989; Einsiedl et al., 2007; Hertkorn et al., 2006; Lam et al., 2007) appeared inconspicuous on visual inspection but revealed systematic intensity distortions which precluded facile computation of meaningful methylene (CH_2) and

N. Hertkorn et al.

Title Page

Abstract | Introduction

Conclusions | References

Tables | Figures

◀ | ▶

◀ | ▶

Back | Close

Full Screen / Esc

Printer-friendly Version

Interactive Discussion

methyl (CH_3) subspectra by means of linear combination (Fig. 5). These were most likely caused by intrinsic variations of $^1J_{CH}$ in CH, CH_2 and CH_3 chemical environments of marine DOM. This applied for ^{13}C DEPT NMR spectra acquired with both QCI and QCO probeheads.

All DOM showed similar overall ^{13}C NMR resonance envelopes typical of an intricate mixture of natural organic matter with noticeable peaks of anomerics and C-aromatics for surface DOM whereas oxygenated aromatics and ketones were of too low abundance to result in noticeable humps at the S/N ratio provided (Fig. 4). Exceptional S/N ratio allowed apodization with weakly attenuating exponential multiplication (Fig. 4A) to reveal groups of sharp NMR resonances helpful to elucidate significant clustering of abundant molecular signatures. Integration according to major substructure regimes revealed continual increase of carboxylic acids and ketones from surface to deep marine DOM, reflecting a progressive oxygenation of marine DOM, with concomitant decline of carbohydrate-related substructures (Table 4).

The dominance of carboxylic acids COOH over peptides CONH and esters COOR was independently corroborated by ^1H NMR spectra of marine DOM acquired in dry DMSO-d_6 under exclusion of moisture in which COOH appeared as broad signal near $\delta_H \sim 12.3$ ppm ($\delta_H \sim 11.6\ldots14.7$ ppm), with a remarkably strong increasing abundance from surface to depth (% COOH/total proton NMR integral, FISH: 4.7 %; FMAX: 4.5 %; 200 m: 7.5 %; 5446 m: 12.1 %). The fraction of CONH could not exceed 4 % of total carbon even if all DON would occur as peptides/proteins because the C/N ratio has been found >25 for all four DOM extract (Table 1). Exclusive occurrence of all marine DON as peptides is, however, an unlikely presumption (McKee and Hatcher, 2010; Maie et al., 2006); see also discussion of sp^2-hybridized carbon in marine DOM. In addition, ^1H NMR spectra of marine DOM in dry DMSO-d_6 revealed at least three chemical environments of ammonium ($^{14}NH_4^+$) near $\delta_H \sim 7.07$ ppm with an ostentatious coupling between ^{14}N and ^1H ($^1J_{NH} = 51.2$ Hz; 1:1:1 triplet, because of nuclear spin for $^{14}N = 1$; % $^{14}NH_4^+$ signal/total proton NMR integral, FISH: 0.8 %; FMAX: 0.6 %; 200 m: 0.6 %; 5446 m: 0.9 %). Furthermore, upper limits for carbonyl carbon derived from

methyl esters ($\delta_C \sim 51\ldots 54$ ppm; Table 4, Fig. 4) were lower than one third of the ^{13}C NMR COX resonance. It is noteworthy that esters more likely survive SPE conditions rather than the drastic chemical alteration imposed by the IHSS humic substances extraction protocol.

Carbohydrate related NMR resonances (i.e. H<u>C</u>O and H<u>C</u>O$_2$ groups) decreased from surface to deep DOM in line with the expectation that these labile constituents will be more easily degraded with increasing DOM age. A certain section of carbon NMR resonances with $\delta_C \sim 70\ldots 78$ pm (Figs. 4, 5) present in both surface marine DOM was found virtually absent in both deep DOM. Pure aliphatics appeared to have their signature changed in between both surface (FISH and FMAX) and deep DOM (200 m and 5446 m). Aromatics were of little abundance in all DOM, and became more oxidized with increasing water depth. DEPT-90 NMR spectra representing solely methine (CH) carbon showed remarkable increase of aliphatic branching from surface to deep marine DOM: <u>HC</u>C$_3$, the most prominent substructure to represent aliphatic branching, increased from 45.7 % (FISH) to 56.7 % (5446 m) of total methin (Table 4). A notable fraction of methin carbon (CH) resonated at $\delta_C > 140$ ppm, a strong indication for the presence of six-membered N-heterocycles, because simple aromatics, including polycyclic aromatic hydrocarbons very rarely resonate beyond $\delta_C > 140$ ppm (see later discussion of sp^2-hybridized carbon chemical environments in marine DOM).

NMR based reverse mixing model to determine H/C and O/C elemental ratios

A ^{13}C NMR based reverse mixing model (Hedges et al., 2002) served to compute the NMR derived elemental H/C and O/C ratios of the four marine DOM fractions. Seven carbon NMR regions of chemical shift (cf. Table 4) attributed to certain fundamental building blocks with given H/C and O/C ratios (Table 4) were multiplied with their relative carbon abundances to provide the NMR derived H/C and O/C elemental ratios shown in Table 4. Feasible correction for carbon multiplicity as derived from ^{13}C DEPT NMR spectra (Fig. 5) would leave these computed values nearly unchanged: a near

50 % reduction of the H/C ratio for aromatic carbon (to account for the presence of quaternary carbon atoms) would be compensated by an elevated H/C ratio for the proposed HC-O units (presence of $H_2\underline{C}$-O and $H\underline{C}$-O units in the respective chemical shift section) and for the proposed CH_2 units (more methyl than methin carbon was present in the C$\underline{C}$H region of marine DOM).

3.5 JRES NMR spectra of marine DOM

^{1}H, ^{1}H J-resolved (JRES) NMR spectra provided well resolved patterns for all four marine DOM, indicative of rather abundant molecular signatures (Fig. 6). The number of JRES cross peaks declined in the order FMAX > FISH > 200 m > 5446 m, and the adjacent pairs of DOM showed more similarity in JRES cross peak patterns than distant ones implying a rather continual evolution of DOM composition. Remarkably, numerous JRES cross peak have been observed even for the deep 5446 m DOM in which fast transverse NMR relaxation has strongly attenuated COSY cross peaks (cf. Fig. 7G, H). A rather large proportion of surface marine DOM (FISH and FMAX) methyl groups (δ_H < 1.6 ppm) was connected to methin (CH; produced doublets in F1) rather than to methylene (CH$_2$; only a few triplets recognizable). With increasing water depth however, the fraction of methyl groups bound to methylene markedly increased and then dominated the upfield chemical shift range of pure aliphatics at δ_H < 1.1 ppm (Fig. 6H). Rather isolated methyl groups, perhaps adjacent to quaternary carbon, with a few small vicinal $^3J_{HH}$ couplings appeared most prominent in FMAX and 200 m samples (δ_H ~ 1.5 ppm). Analogous considerations applied to methoxy groups near δ_H ~ 3.3...3.7 ppm with strong centered JRES cross peaks with tiny couplings ($^3J_{HH}$ < 2 Hz) which appeared in the order FMAX > FISH ≥ 200 m > 5446 m, thereby corroborating assignment from DEPT HSQC NMR spectra (Figs. 8, 9), which discriminated between aliphatic methyl esters and ethers, with $^4J_{HH}$ for methyl ethers and $^5J_{HH}$ for methyl esters, respectively. The complex spin systems characteristic of carbohydrates and other extended spin systems declined in the order FMAX > FISH > 200 m > 5446 m. The section of unsaturated protons (δ_H > 5.5 ppm) showed several olefinic protons with small

$^{n}J_{HH}$ couplings ($\delta_H \sim 6.2$ ppm, $^{n}J_{HH} < 3$ Hz), likely from olefins at aliphatic ring junctions with restricted conformational mobility; others showed COSY cross peaks to other olefinic protons (Supporting Online Fig. 4A, C). Similar signatures have been previously recorded in ^{1}H NMR spectra of ultrafiltered marine organic matter (Hertkorn et al., 2006; Fig. 2) and sediment extracts (data not shown). Large vicinal scalar couplings ($^{3}J_{HH} > 7$ Hz) from $\delta_H \sim 6.7\ldots7.6$ ppm indicated α, β-unsaturated olefins present in all marine DOM.

3.6 COSY NMR spectra of marine DOM

The COSY NMR spectra of surface DOM samples FISH and FMAX displayed many hundreds of intense cross peaks and slightly lesser counts of barely visible ones. Both COSY NMR spectra shared approx. 75 % of their intense cross peaks in the aliphatic section (Fig. 7, Supporting Online Figs. 3, 4 and 5), whereas only slightly more than half of the observed aromatic COSY cross peaks were common to both NMR spectra. About 4500 COSY off-diagonal cross peaks appeared resolved in sample FMAX of which ~85 % derived from sp^3-hybridized carbon ($\underline{H}C_{sp^3}$-$C_{sp^3}\underline{H}$, $\underline{H}C_{sp^3}$(O)-$C_{sp^3}\underline{H}$, and $\underline{H}C_{sp^3}$(O)-C_{sp^3}(O)$\underline{H}$) and the remainder from sp^2-hybrized carbon ($\underline{H}C_{sp^2}$-$C_{sp^2}\underline{H}$; $\delta_H > 5$ ppm). Corrected for symmetry across the diagonal (50 %) and average spin system size (~3.5 protons per spin system; approximate value), the COSY signature in marine DOM sample FMAX suggested the presence of several hundreds of individual "signature" molecules of either biochemical or biogeochemical origin. In general, the COSY NMR spectrum of FMAX showed about 25 % more abundant cross peaks than that derived from FISH. This remarkable richness of COSY cross peaks in marine DOM is unprecedented because meaningful COSY NMR spectra of marine organic matter have not been acquired previously. It appears that marine DOM isolated by means of SPE exhibit in part larger extents of slow NMR relaxation (that enabled the acquisition of high resolution COSY NMR spectra) than those derived from ultrafiltration or by the IHSS extraction protocol. Recent studies suggest that SPE based DOM

isolation of marine waters discriminates against carbohydrates, e.g. in comparison with marine DOM isolated by means of ultrafiltration and especially ROED, the combination of reserve osmosis (RO) and electro dialysis (ED), which currently provides the highest carbon yield of all methods employed for isolation of marine DOM (Koprivnjak et al., 2009).

With increasing water depth, the observed COSY signature of marine DOM became progressively attenuated; this specifically applied for the 200 m and 5446 m DOM samples. However, the position of all major aliphatic COSY cross peaks of DOM samples 200 m and 5446 m agreed with strong COSY cross peaks observed DOM for the samples FISH and FMAX.

Given the appreciable conformity of one-dimensional ^{1}H NMR spectra (Fig. 3, Supporting Online Figs. 1 and 2) and discernible COSY cross peak positions for all four DOM samples, the disappearance of COSY signatures in the sample order FMAX ~ FISH > 200 m > 5446 m most likely related to ever increasing prevalence of fast transverse relaxation for which two mutually non-exclusive and possibly cooperative mechanisms can be suggested. The first relates to a prospective growing size of marine DOM molecules with increasing age at depth (the ^{14}C age places a minimum constraint on DOM turnover since successive reworking of aged DOM in the deep ocean will not modify the apparent ^{14}C age of DOM). Larger molecules of lesser atomic mobility, which could show compositions and structures similar to their smaller precursors could not to be easily differentiated by means of their 1-D NMR spectra. Notably, FTICR mass spectra of Atlantic Ocean DOM showed both increased average mass, with a however small displacement by about 10 Dalton, and a relative increase of unsaturation (Flerus et al., 2011a). Alternatively, the continual incorporation of metals into the sizable DOM molecules which typically exhibit multiple oxygen-, nitrogen- and sulphur-derived functional groups capable of forming coordination compounds with metal ions would lead to fast NMR relaxation. The likelihood to incorporate and retain metals grows with molecular size of NOM because of better opportunities to form chelating coordination compounds with large binding constants. Long ocean residence

High field NMR spectroscopy and FTICR mass spectrometry

N. Hertkorn et al.

Back | Close

Full Screen / Esc

Printer-friendly Version

Interactive Discussion

time of DOM may induce progressive metal complexation because metal ions with lesser binding constants will increasingly become displaced by such with stronger binding constants (e.g. higher charged and kinetically stable metal ions) (Vraspir and Butler, 2009; Witter et al., 2000).

5   It is furthermore conceivable that the apparent similarity of COSY NMR spectra from both surface and deep DOM, and the distinction between these two sets of samples (cf. also Fig. 16) reflects increasing molecular diversity with ocean depth (and DOC age) caused by increased fractions of (extensively re-worked) biogeochemical molecules present in deep DOM. These could have originated from more diffuse sources through-
10   out the entire ocean column, produced on average with longer timescales than those from surface biochemical reactions. Here, increase in molecular diversity (gain in entropy) would diminish NMR signatures in deep DOC because smaller numbers of molecules would exceed a certain minimum concentration required to produce visible COSY cross peaks. Then, the cross peak integral would extend to larger areas with
15   lesser disposable S/N ratio for individual COSY cross peaks.

3.7 Comparison of homonuclear 2-D NMR spectra of marine DOM (JRES, COSY and TOCSY NMR spectra)

The excellent COSY NMR cross peak resolution of marine DOM was not readily available in TOCSY NMR spectra (Figs. 2, 13). At first, more numerous cross peaks with
20   higher S/N ratio were expected in TOCSY than in COSY NMR spectra. However, the superposition of abundant in-phase TOCSY cross peaks almost completely filled the entire accessible area of chemical shift with a near continuous assembly of cross peaks, especially in the aliphatic section (i.e. from $\delta_H \sim 0.5\ldots4.5$ ppm; Figs. 2B, 13A–D). The application of strongly apodizing functions in F1 and F2 of TOCSY NMR spec-
25   tra resulted in considerably enhanced apparent resolution, primarily for -O-**H**C-**H**C-O- and aromatic cross peaks (Fig. 2C, D). However, purely aliphatic cross peaks then became somewhat blurred and showed lesser definition than COSY cross peaks, likely a consequence of superposition of very many aliphatic cross peaks of minor abundance

(in part from higher order spin systems), overlaid with vertical T_1 noise from spectrometer instabilities and parallel diagonals from thermal noise.

JRES NMR spectra, on the other hand, produced fewer numbers of cross peaks than both COSY and TOCSY NMR spectra for several reasons. At first, the overall nominal resolution of JRES NMR spectra was only <1/300 compared with that of COSY and TOCSY NMR spectra (cf. Table 2) and hence allowed for a far lesser disposable peak dispersion. In addition, the long duration of F1 increments in JRES NMR spectra (here: 10 ms as opposed to TOCSY: 104 µs and COSY: 104 µs) imposed mandatory loss of magnetization from prolonged operative NMR relaxation at high F1-resolution. In fact, the discretionary resolution of JRES NMR spectra obtained from DOM was limited to detect spin spin couplings $^nJ_{HH} > 2.5$ Hz (Fig. 6), considerably larger than active and passive J_{HH} operating in COSY and TOCSY NMR spectra of DOM. Furthermore, a shorter total acquisition time of JRES as compared with COSY/TOCSY NMR spectra (because of limited useful numbers of F1 increments) will accumulate a lesser overall S/N ratio, attenuating weak cross peaks even further. Hence, JRES NMR spectra were only capable to depict abundant molecular signatures in marine DOM, whereas COSY NMR spectra were (and will be in future) best suited to reveal diversity of organic composition. TOCSY NMR spectra on the other hand will be best suited to reveal faint NMR signatures of low abundance like those derived from unsaturated biogeochemical mixtures (cf. discussion of sp^2-hybridized carbon in marine DOM).

3.8 DEPT HSQC NMR and HSQC TOCSY NMR spectra of marine DOM

The expansive aliphatic HSQC cross peak of all four DOM samples (Fig. 14, cf. also Fig. 10), which represented superimposed **HC**-C and **HC**-X (X: O, N, S) chemical environments, lacked peak discrimination which could be vastly improved by spectral editing according to carbon multiplicity. The combination of methyl- and methylene-selective DEPT-HSQC NMR spectra revealed well resolved cross peaks for all three types of protonated carbon, i.e. CH_3, CH_2 and CH, although with decreasing amplitude (Fig. 8). Effects of differential relaxation influenced relative peak amplitudes in CH_2-

and CH$_3$-edited DEPT HSQC NMR spectra without affecting the significance of cross peak assignments. Methyl groups bound to carbon (C-CH$_3$), sulphur (S-CH$_3$), nitrogen (N-CH$_3$) and oxygen (O-CH$_3$) occupied different sections of chemical shift which were unambiguous for the latter two and rather extended for C-methyl groups. S-CH$_3$
5 groups and methyl attached to olefins resonated in the same chemical shift region and were potentially superimposed (Fig. 9A). Methoxy groups could be discriminated into aliphatic and at most a few aromatic methyl esters and aliphatic methyl ethers according to their specific chemical shift regions (Fig. 9C). Methyl groups terminating non functionalized aliphatics, like e.g. peptide side chains resonated at $\delta_H < 1$ ppm and con-
10 stituted a small minority (approx. 15 %) of methyl found in all marine DOM investigated here. Downfield chemical shift displacement of methyl cross peaks caused by chemical shift anisotropy from proximate carbonyl derivatives, which is favored in alicyclic rings because of abundant short range connectivities, was rather common and responsible for the bulk of C-**CH**$_3$ NMR cross peaks in the region of $\delta_H \sim 1.0\ldots1.6$ ppm.

15 ## 3.9 HMBC NMR spectra of marine DOM

HMBC NMR spectra acquired from surface DOM samples FISH and FMAX showed extensive ($\sim$80 %) conformity of HMBC cross peak patterns with excellent NMR cross peak dispersion. The relatively low sensitivity of HMBC NMR spectra (Table 2) (Crouch et al., 2001) precluded so far the acquisition of meaningful HMBC spectra of deep
20 marine DOM 200 m and 5446 m, respectively. HMBC cross peaks indicated numerous complex aliphatics with (**H**C(C)**C**O) and without oxygen (**H**C(C)**C**C), indicative of alkylated and standard carbohydrates (with anomeric CH pairs) and unsaturated (i.e. olefinic and aromatic) and carbonyl carbon with a broad range of C- and oxygenated alkyl substitution. HMBC cross peaks are less sensitive than HSQC and homonu-
25 clear (^{1}H, ^{1}H) NMR cross peaks (Table 2) but showed superior connectivity information, enabling the assembly of extended spin systems across quaternary carbon and heteroatoms. In future, separate studies, HMBC cross peaks will be very valuable

for assignment confirmation of relatively abundant molecular signatures proposed by COSY and other NMR spectra.

3.9.1 Structural detail of carboxyl-rich alicyclic molecules (CRAM) in marine DOM

Marine DOM appears at first composed of four major constituents: peptides/proteins, carbohydrates, lipids and thermogenic organic carbon (TMOC). The latter originates from thermal decomposition of organic compounds via a succession of complex chemical degradations under harsh conditions which from the onset have largely obviated significant biogenic signatures. In contrast, peptides and carbohydrates are commonly well related to biogenic precursors. Lipids, a rather diverse class of molecules (Graeve and Janssen, 2009; Lipp and Hinrichs, 2009; Cane and Ikeda, 2011) have been extensively processed in marine waters to eventually result in abundant carboxyl-rich alicyclic molecules (CRAM), itself a very complex mixture (Hertkorn et al., 2006; Lam et al., 2007), thereby resembling TMOC. CRAM have been first elucidated from ultrafiltered marine organic matter (UDOM) (Hertkorn et al., 2006) and were shown to contain an unusually large fraction of carboxylic acids, not found in any (except a very few) known natural products of appreciable size (e.g. >450 Da, a typical size for marine DOM as deduced from FTICR mass spectra).

^{13}C NMR spectra place stringent restrictions on the occurrence and structural characteristics of marine DOM constituents (Table 4). TMOC abundance in marine DOM as deduced from ^{13}C NMR spectra likely ranged below 2 % of total carbon (Dittmar and Koch, 2006), considering the fact that olefinic carbon in marine DOM was found more abundant than aromatic carbon. If we regard the CCH and COX substructures as characteristic of CRAM, its content in marine DOM ranged from 51 % (DOM sample FISH) to 56 % (DOM sample 5446 m). Again, a very large ratio of carboxylic acids (and some methyl esters; Fig. 9C) to total (CRAM-derived) carbon has been found in CRAM, ranging from 0.28:1 (DOM sample FISH) to 0.33:1 (DOM sample 5446 m). Hence, COX groups had to be proximate to many aliphatic carbon atoms for simple reasons of

Title Page

Abstract | Introduction

Conclusions | References

Tables | Figures

◄ | ►

◄ | ►

Back | Close

Full Screen / Esc

Printer-friendly Version

Interactive Discussion

abundance. Alicyclic geometry with its more numerous pathways of connections between pairs of atoms favoured relative proximity (i.e. small minimum numbers of connecting chemical bonds between arbitrary pairs of atoms) even more. Methyl-edited DEPT HSQC NMR spectra (Fig. 9B) demonstrated abundant proximity of aliphatic methyl groups (C**CH**$_3$ units) and carbonyl derivatives, because the short range chemical shift anisotropy of the carbonyl group operated on approximately 70 % of aliphatic methyl, inducing downfield chemical shifts from $\delta_H \sim 1.0\ldots1.6$ ppm (Fig. 9A). Classical aliphatic methyl groups, like peptide side chains and common lipids, resonating at $\delta_H < 1.0$ ppm, contributed less than 15 % to the C**CH**$_3$ NMR integral (Fig. 9A).

Remarkably, methylene edited DEPT HSQC NMR spectra corroborated these findings and showed two major lobes of extended -C-**CH**$_2$-C- NMR cross peaks with nearly identical total cross peak integral, indicating -C-**H**$_2$**C**-C$_z$-COX units with proximate COX (two or less bonds away; $z \leq 1$; Fig. 9B, lobe b) and others indicating -C-**H**$_2$**C**-C-C$_x$-COX units ($x \geq 1$; Fig. 9B, lobe a) with larger minimum distance between methylene carbon and carbonyl derivatives. Lobe b showed slightly larger -C-**CH**$_2$-C- NMR cross peak integral than lobe a; this implies that a majority of the methylene carbon in marine NOM is two or less bonds away from **C**OX (i.e. **C**OX occupies α- or β-position with respect to methylene). In contrast to methyl carbon, methylene carbon offers options of chain elongation in two different directions with a proportionally larger probability of finding (very) proximate COX at otherwise near statistical distribution of functional groups. It is noteworthy that CH$_2$-COX units cannot be part of alicyclic rings.

The carboxylic NMR resonance appeared very similar for all marine DOM, with a maximum intensity near $\delta_C \sim 174.3$ ppm, a near Gaussian intensity distribution across a sizable chemical shift range (range at half height, $\delta_C \sim 171.8\ldots177.6$ ppm), indicating a maximal chemical diversity of COX chemical environments with no visible preference of (remote) substitution. COX from deep DOM 5446 m ranged by 0.5 ppm toward lower field with a maximum δ_C of 175 ppm and a chemical shift range at half height of $\delta_C \sim 171.8\ldots178.2$ ppm, possibly indicating a larger fraction of purely aliphatic carboxylic groups like those in classical lipids (cf. JRES NMR spectra; Fig. 6H). In contrast,

Title Page

Abstract | Introduction

Conclusions | References

Tables | Figures

◀ | ▶

◀ | ▶

Back | Close

Full Screen / Esc

Printer-friendly Version

Interactive Discussion

ultrafiltered marine DOM showed two major carboxylic acid peaks, one broad hump with maximum amplitude at $\delta_C \sim 177$ ppm and a relatively sharp NMR resonance of lesser integral centred at $\delta_C \sim 175$ ppm, which was assigned originating from carboxylated carbohydrates (Hertkorn et al., 2006). The absence of the relatively sharp ^{13}C NMR resonance in SPE derived marine DOM implies an extraction selectivity of SPE on one hand and of ultrafiltration on the other. Solid-state NMR spectra of RO/ED derived marine organic matter also did not show this relatively sharp ^{13}C NMR resonance, perhaps in part because of intrinsic low resolution of solid state NMR spectroscopy.

3.9.2 Depiction and analysis of less common sp^2-hybridized carbon in marine organic matter

Hydrogen atoms bound to sp^2-hybridized carbon [i.e. olefinic and aromatic carbon chemical environments (carbonyl derivates do not have directly bonded hydrogen except for aldehydes)] in marine DOM typically accounted for less than 5 % of non-exchangeable proton NMR integral and occupied the chemical shift range of $\delta_H \sim$ 5...10 ppm, with small contributions of anomeric protons at $\delta_H < 5.5$ ppm (Fig. 3, Table 3).

Unsaturated carbon chemical environments in marine DOM have been recognized by means of proton and carbon 1-D NMR spectra (Hertkorn et al., 2006; Lam et al., 2007; Aluwihare et al., 2002) but not further characterized by NMR spectroscopy because of lack of sensitivity. UV/VIS spectra have supplied decisive clues about chromophoric (light absorbing) and light emitting (fluorescent) molecules in marine DOM (colored dissolved organic matter, CDOM) (Coble, 2007) and thereby provided identification of selected sp^2-hybridized carbon in aromatics (phenols, quinones, pyrrols), olefins, carbonyl derivatives and α, β-unsaturated (polarized) double bonds, respectively.

Prospective isolated olefins in marine DOM likely originate from natural products such as common unsaturated lipids derived from unsaturated fatty acids and sterol derivatives. Conjugated olefins occur in linear terpenoids which have been proposed

in freshwater DOM (Lam et al., 2007) but commonly occur in marine waters as well (Blunt et al., 2010). A rich diversity of natural products contains α, β-unsaturated molecules, often in conjunction with aromatics (Blunt et al., 2010). Amide moieties in peptides/proteins as well as in amino sugars are common contributors to carbonyl derivatives in marine DOM.

Classical aromatic molecules in marine DOM comprise oxygenated, hydroxylated and carboxylated single and small condensed aromatics (Dittmar and Koch, 2006; Dittmar and Paeng, 2009; Hatcher et al., 2005); lignin-derived phenols detected in marine DOM are much less abundant than in soil DOM which primarily derives from vascular plants with abundant lignin (Rezende et al., 2010). Nitrogen heterocycles in marine DOM comprise pyridine derivatives (Maie et al., 2006) as natural products and heterocycles with up to several incorporated nitrogen atoms like those occurring in DNA derivatives; nitrogen, sulphur and oxygen in five-membered aromatic rings are further feasible candidates for sp^2-hybridized carbon in marine DOM (Blunt et al., 2010).

Another, more complex assembly of sp^2-hybridized carbon in marine DOM with considerable average ^{14}C age derives from black carbon (Masiello, 2004), which ultimately might originate from (natural and anthropogenic) terrestrial burning and biogeochemical weathering (Dickens et al., 2004) transported into the sea via riverine transport (Battin et al., 2009) and atmospheric deposition (Masiello and Druffel, 1998), and from deep see infusion by hydrothermal vents and other petrogenic, more diffuse sources. Thermogenic marine carbon (TMOC) has been found widely distributed in the ocean and accounts for up to several percent of total marine organic carbon (Dittmar and Koch, 2006), elevating TMOC to a significant proposed constituent of total marine organic carbon. The abundance of TMOC in the ocean correlates passively with marine salinity (Dittmar and Paeng, 2009), suggesting preferential photochemical degradation as the major sink of TMOC (Dittmar and Paeng, 2009).

TMOC in marine DOM has at first been identified in FTICR mass spectra because of prevalent hydrogen deficient molecules with a large aromaticity index (Koch and Dittmar, 2006) which cannot be easily explained to have resulted from biochemical

High field NMR spectroscopy and FTICR mass spectrometry

N. Hertkorn et al.

precursors. TMOC is likely composed of (condensed) aromatic units like oxygenated and carboxylated polycyclic aromatic hydrocarbons with a few to several contiguous aromatic rings (Hockaday et al., 2006; Dittmar and Koch, 2006; Cheng et al., 2006). Here, appreciable ranges of O/C ratios as deduced from FTICR mass spectra will re-
5 sult in variable carbon oxidation states (Kroll et al., 2011; Cheng et al., 2006), and electronic long-range interactions across extended π-systems (Bauschlicher et al., 2009) will cause different extents of aromaticity (and reactivity) of individual bonds within nominal benzene rings (Aihara et al., 2011). In NMR spectroscopy, carboxylation will induce downfield chemical shifts in both proton and carbon NMR (Perdue et al., 2007). In con-
10 trast, oxygenation will induce sizable upfield chemical shifts in both proton and carbon NMR because of strong electron-donating effect in ortho and para positions (Perdue et al., 2007). Owing to extensive conjugation and strong resonance, these cumulative chemical shift effects can operate in remote positions (up to 4–6 bonds away) and are therefore difficult to predict in complex molecules. The intrinsic heterogene-
15 ity of this inhomogeneous class of TMOC molecules resembles that of carboxyl-rich alicyclic molecules (CRAM), another key contributor of marine DOM (Hertkorn et al., 2006; Lam et al., 2007) and will manifest itself in rather low-resolution NMR signatures (i.e. extended NMR cross peaks in two-dimensional NMR spectra). One-dimensional (^{1}H and ^{13}C) NMR spectra alone will not allow unambiguous structural identification
20 of TMOC because of overlap from nitrogen heterocycles and other strongly electron withdrawing aromatics.

NMR chemical shifts of pure aromatic hydrocarbons occupy a relatively narrow range of ^{13}C chemical shifts irrespective of structural arrangements and degree of condensation: protonated carbons range from $\delta_C \sim 120 \ldots 135$ ppm while quaternary carbons
25 resonate from $\delta_C \sim 135 \ldots 143$ ppm (Hansen, 1979). In contrary, proton chemical shifts in pure polycyclic aromatic hydrocarbons are rather sensitive to specific steric arrangements. Normal, uncongested hydrogen positions resonate from $\delta_H \sim 7 \ldots 8$ ppm, depending on position and extent of condensation: larger PAH superimpose several deshielding ring currents, resulting in progressive downfield proton NMR chemical

shifts. Sterically congested bay and fjord regions impose downfield proton NMR chemical shift depending on the extent of steric hindrance: most pronounced steric congestions in narrow fjord regions produce downfield proton chemical shifts beyond 9 ppm, lesser tight bays like those related to incorporated five-membered rings resonate from $\delta_C \sim 8.6 \ldots 8.9$ ppm (Tominaga et al., 2011; Williamson et al., 1986).

However, major substructure regimes within the thermogenic signature of marine DOM can be proposed with predictable NMR chemical shift characteristics (Fig. 12). ^{1}H,^{1}H TOCSY and ^{1}H, ^{13}C HSQC NMR experiments are most appropriate to probe marine DOM signatures of low abundance because their absorptive lineshape allows superposition of small individual NMR resonances into aggregated cross peaks which can be processed with adapted apodization function to enhance their apparent S/N ratio (Figs. 2, 13, 14). Electron-deficient six-membered nitrogen heterocycles produce strong proton and carbon NMR downfield shifts; plausible candidates in marine DOM include natural products derived from pyridine, indole and histidine and more complex compounds derived from nucleic acids and analogues. In contrast, aromatic amines and simple five-membered N-heterocycles, as plausible candidates of chlorophyll degradation, exhibit considerable proton and carbon NMR upfield shifts because of electron-donating capacity.

3.10 Conceptual model and NMR chemical shift characteristics for polycyclic aromatic chemical environments of thermogenic origin (TMOC) in marine DOM

A conceptual model to depict the effects of conceivable substitution patterns in black carbon analogous marine thermogenic carbon was proposed in Fig. 12A (atom numbering and computed ^{1}H and ^{13}C chemical shifts, cf. Supporting Online Fig. 5 and Supporting Online Table 2). This model denoted the effects of relative steric congestion (Fig. 12A, PAH narrow and open bay regions A1–A3 and B1–B2), relative condensation (Fig. 12A, substructure D; see also relative downfield ^{1}H NMR chemical shifts of B2 compared with B1 because of larger aromatic ring current from more extended

condensation; Supporting Online Table 2) in unsubstituted PAH hydrocarbon environments as well as the consequences of substitution with plausible electron-withdrawing (-COOH, N-heterocycles; substructures E1 and E3) and electron-donating (-OH; substructures E2) substituents that may exhibit long-range transmission of NMR-relevant substituent effects across conjugated π-systems.

Within common edge moieties of unsubstituted PAH, steric congestion of proton pairs (Bauschlicher et al., 2009; Tominaga et al., 2010) decreases from narrow fjord regions A (substructures A1, A2, A3) through mid-bay sections B (substructures B1, B2) through unhindered domains C (substructures C1 and C2). Extensive steric congestion (substructures A1 ~ A2 ~ A3 > B1 ~ B2) imposes progressive downfield shift beyond $\delta_H > 9$ ppm whereas δ_C sustains considerably less relative chemical shift displacement (atom pairs 24/46 as compared with 25/26; cf. Supporting Online Fig. 5, Supporting Online Table 2). Lesser steric hindrance in open bays (sections B) imposed mid-size downfield shifts ($\delta_H \sim 8.6$ ppm) at nearly unaltered δ_C (atom pairs 27/49; cf. Supporting Online Fig. 5). Similarly, increased aromatic condensation which implies superimposed and amplified in-plane deshielding ring currents (Williamson et al., 1986; Tominaga et al., 2010), imposes downfield proton chemical shift (atom pairs 44/25; 44(42)/25; cf. Supporting Online Fig. 5). Increased condensation implies more numerous long range carbon-carbon contacts within four bonds and here, downfield shifts of δ_C may occur (atom pairs 17/23: $\Delta\delta_C \sim 11$ ppm and 16/22: $\Delta\delta_C \sim 1$ ppm; cf. Supporting Online Fig. 5, Supporting Online Table 2).

Heterocyclic nitrogen incorporated into six-membered rings imposes electron-withdrawal and strong deshielding for both δ_H and δ_C [cf. $\delta_{C5/H5} = 154.6/9.90$ ppm (fjord region A1), $\delta_{C2/H2} = 164.3/9.18$ ppm]. In fact, this combination of pronounced proton and carbon downfield chemical shift might serve as a recognition feature for six-membered N-heterocycles because protonated carbons (methins) in any polycyclic aromatic hydrocarbon rarely resonate beyond $\delta_C \sim 140$ ppm (Hansen, 1979). This even applies in case of additional carboxylic substitution (section E1) which rather imposes significant δ_H downfield displacement for ortho- and para-positions while barely

affecting δ_C. In contrast, electron-donating substituents like hydroxyl or ethers (section E3) which act upon ortho- and para-positions as well, are mandatory to displace δ_C to <120 ppm; similarly, δ_H < 7 ppm imply presence of oxygen attached to, or incorporated into six-membered rings within PAH (Perdue et al., 2007).

In conclusion, pure hydrocarbon PAH exhibit variable proton chemical shift in dependence of steric crowding and degree of condensation, both of which induce sizable proton NMR downfield chemical shift while leaving δ_C nearly unchanged. Six membered N-heterocycles will show combinations of downfield chemical shift for protons and carbon not available by any means of electron withdrawing and -donating oxygenation of aromatic hydrocarbons. Here, electron widthdrawing substitution (COOH, COOR, CONH) will displace ortho as well as para positions to lower field for both δ_H and δ_C whereas electron donating substitution will displace ortho and para positions to higher field in both δ_H and δ_C. At first approximation these effects can be considered near additive as known as from NMR increment analysis (Perdue et al., 2007).

3.11 NMR characterization of unsaturated chemical environments in marine DOM

3.11.1 TOCSY NMR spectra

The distinctive sensitivity of TOCSY NMR spectra was perfectly eligible to detect minor and possibly diffuse NMR signatures in less congested spectral regions. Hence, TOCSY cross peaks were ideally suited to determine chemical environments of hydrogen attached to sp^2-hybridized carbon in the chemical shift range of $\delta_H \sim 5 \ldots 10$ ppm. Their relative fast transverse NMR relaxation caused by enhanced contributions from chemical shift anisotropy (CSA) suggested the use of apodization functions which improved the S/N ratio at the expense of resolution (Fig. 2) to reveal weak and extended NMR signatures of complex biogeochemical mixtures like those of TMOC (Fig. 13). Accordingly, high-field NMR spectra have uncovered otherwise elusive extended downfield olefinic and aromatic TOCSY cross peaks in marine DOM which provided useful constraints about chemical environments of sp^2-hybridized carbon (Fig. 13).

3.11.2 HSQC NMR spectra

The strength of HSQC NMR spectra, which exhibit shorter duration and hence less susceptibility of magnetization loss from fast transverse NMR relaxation than DEPT HSQC NMR spectra, resides in the detection of low abundant features, in particular when acquired at high S/N ratio with limited F1 resolution and apodization designed for S/N enhancement. Unsaturated chemical environments in marine DOM contain almost exclusively methine and quaternary carbon; terminal methylene ($C=CH_2$), while present in some marine natural products (Blunt et al., 2010), is rather elusive in natural organic matter. Hence, spectral editing is of limited use in the HSQC chemical shift section of sp^2-hybridized carbon ($\delta_C > 90$ ppm). All four marine DOM samples revealed significant HSQC cross peaks of unsaturated carbon chemical environments (Fig. 14). Interestingly, transverse relaxation accelerated markedly from surface to deep DOM, requiring disproportionally large numbers of scans to acquire meaningful HSQC NMR spectra of deep (5446 m) marine DOM (Supporting Online Table 1).

3.11.3 Joint HSQC and TOCSY cross peak assignment of marine DOM

Both TOCSY and HSQC NMR spectra of marine DOM shared the same proton NMR chemical shift but indicated different units within: HSQC NMR cross peaks indicated any CH_n-X group (n: 1, 2, 3; X: any atom) with directly bound carbon-proton pairs (magnetization transfer via $^1J_{CH}$) whereas TOCSY NMR cross peaks required rather proximate coupled proton pairs (magnetization transfer via $^nJ_{HH}$; n ~ 2...5). Saturated molecules with large H/C ratios will exhibit abundant HSQC and TOCSY cross peaks, whereas fused aromatic rings and hydrogen deficient molecules in general will display HSQC cross peaks for any C-H pair even when isolated, but only a few to none TOCSY cross peaks in case of isolated protons (similar considerations applied to the appearance of COSY and JRES cross peaks). Furthermore, individual carbon and hydrogen atoms at polarized double bonds might resonate at widely different HSQC as well as TOCSY cross peaks positions. Olefins and aromatics with extensive aliphatic

Title Page

Abstract | Introduction

Conclusions | References

Tables | Figures

◀ | ▶

◀ | ▶

Back | Close

Full Screen / Esc

Printer-friendly Version

Interactive Discussion

substitution are in general sterically protected from attack, making them likely candidates for survival especially in aged deep water DOM. Nevertheless, the proposed HSQC and TOCSY cross peak assignments of sp^2-hybridized carbon in marine DOM (Figs. 13, 14) were in mutual agreement.

3.12 FTICR mass spectra of marine DOM

Ultrahigh resolution Fourier transform ion cyclotron mass spectra (FTICR/MS) of Atlantic Ocean SPE-DOM each provided several thousands of mass peaks (Koch et al., 2005; Kujawinski et al., 2009), of which many hundreds could be assigned to extended CHO, CHNO, CHOS and CHNOS molecular series (Fig. 15 and Table 5) based on excellent mass accuracy and mass resolution. From surface to deep DOM, slightly increasing numbers of mass peaks occurred of which similar fractions (near 45 %) were assigned to molecular formulas (Table 5). The relative oxygen content derived from intensity weighted assigned mass peaks was near 36 % for the three near surface samples and 42 % for the deep sample 5446 m. This increase of oxygen caused the relative carbon content to decrease from typically 50–52 % (slightly increasing from surface with increasing depth) to 47 % in case of the deep sample 5446 m. Consequently, the computed H/C ratio increase for this deep sample was likely an indirect consequence of enhanced oxygenation rather than increase of saturation.

The abundance of CHO and CHNO molecular series grew from surface to bottom DOM, whereas CHOS and especially CHNOS molecular series markedly declined. Visual inspection of entire FTICR mass spectra revealed minor alterations of peak distributions, with extended continual series and a very few large intensity mass peaks, least abundant in the 200 m sample and likely indicative of biological origin. The average mass grew by about 10 Da from surface to deep DOM. This at first inconspicuous looking change might reflect in fact major alterations of molecular composition and structure within the various marine DOM. Any single marine DOM mass peak represented many isomers, possibly hundreds to thousands of them were projected onto any given mass peak (Hertkorn et al., 2008). This superposition corresponded to a

massive intrinsic averaging and considerable alterations of DOM structure were required to effect in essence marginally looking mass shifts. Expansion of nominal mass sections which were well suited to depict organic molecular diversity (Hertkorn et al., 2008) demonstrated a decline in abundance of extensively unsaturated (i.e. aromatic) CHOS compounds from surface to bottom DOM at otherwise similar mass peak distributions.

The main dissimilarities denoted in van Krevelen diagrams of marine DOM with depth were observed within the ratios $0.5 < H/C < 1.5$ and $O/C < 0.3$ and primarily concerned medium unsaturated CHOS and CHNOS molecules. Accordingly, the numbers of (mostly CHO and CHNO) molecules denoted within the ratios $0.65 < H/C < 1.7$ and $0.25 < O/C < 0.7$ were higher in case of deep marine DOM (200 m and 4556 m) than in the top layer DOM (5 m and 48 m). Furthermore, the counts of oxygen atoms in CHO, CHNO and CHOS molecular series increased from top to bottom DOM, indicative of progressive oxidation, in line with the NMR results (Table 4).

Cluster analysis, based upon relative intensities of assigned mass peaks, revealed at first decreasing similarity of marine DOM with growing difference in water depth indicative of a continual DOM evolution from surface to deep water (Fig. 16; cf. also proton NMR spectra, Fig. 3; Supporting Online Fig. 2). Comparison of consolidated pairs of surface (5 m and 48 m) and deep (200 m and 5446 m) DOM mass spectra revealed additional striking compositional variance. Surface DOM was enriched in certain oxygen-deficient CHOS and CHNOS molecules (O/C ratio <0.3), with CHOS molecules showing larger H/C ratios than CHNOS molecules. This surprising behaviour (nitrogen carries indirect hydrogen into molecular formulas: i.e. a NH fragment can be inserted into any C-C and C-H bond but not N alone) implied that CHNOS molecules in surface marine DOM were "even" more unsaturated than CHOS molecules; i.e. they likely contained heterocyclic nitrogen. The observed oxygen deficiency within these molecular series probably excluded sulfates as significant marine SPE-DOM contributors, which also would exhibit considerable water solubility and therefore poorly absorb on PPL resin.

On the contrary, consolidated deep (200 m and 5446 m) marine DOM contained larger counts of specific CHO and CHNO molecules of intermediate H/C and O/C ratio, indicative of CRAM but also ranging in part into the aromatic realm (Koch and Dittmar, 2006), alongside with a marginal series of oxygen-deficient CHOS molecules; unique CHNOS molecules in deep DOM were essentially absent. Three CHOS molecules ($C_{18}H_{37}O_6S$, $C_{20}H_{41}O_8S$ and $C_{22}H_{45}O_9S$) were found abundant in consolidated deep ocean DOM (Fig. 16).

The occurrence of oxygen deficient CHOS compounds in surface DOM could be partly explained by integration of reactive, photoproduced reduced sulfur species such as hydrogen sulfide (H_2S), dimethylsulfide [$(CH_3)_2S$], carbonylsulfide (O=C=S) into functionalized molecules (Andreae and Crutzen, 1997; Amrani et al., 2007; Pos et al., 1998) under conditions of photochemistry and possibly metal catalysis, assisted by mineral atmospheric deposition (Paytan et al., 2009).

3.12.1 NMR and FTMS derived H/C and O/C elemental ratios

Both NMR and FTICR derived H/C and O/C elemental ratios for themselves occupied rather narrow bandwidths but differed by about 0.25 units for H/C and less than 0.2 units for O/C ratios (Tables 4 and 5). The proposed NMR mixing model to compute elemental ratios (Table 4) appeared reasonable and the observed displacement of FTMS derived molecular compositions toward decreased apparent oxidation seemed to contradict the conventional wisdom that ESI ionization will discriminate in favour of oxygenated compounds relative to, e.g. hydrocarbons (Hertkorn et al., 2008). Carbohydrates in marine DOM, while unambiguously established by NMR signatures, including expansive oxymethylene (OCH$_2$) and anomeric HSQC cross peaks (Figs. 9B, 10), left only minor signatures in the van Krevelen diagrams, where they should have occupied the section of oxidized ($0.8 < O/C < 1.0$) and fairly saturated ($1.7 < H/C < 2.0$) molecular compositions. Carbohydrates in marine DOM were supposedly of higher molecular weight (Ohno et al., 2010), corresponding to a lesser volatility and tendency of getting ionized under ESI conditions. It could be argued that covalent binding of

carbohydrates to other molecules, like peptides (in case of glycoproteins) and lipids (lipopolysaccharides) would have displaced the carbohydrates toward more average H/C and O/C values even if their NMR visible chemical environment would have been preserved. While this might have happened, a faithful representation of all marine

5 DOM molecules by means of FTICR mass spectra would nevertheless have provided average H/C and O/C ratios in some accordance with NMR data. A displacement of the entire MS-derived compositional space toward lesser O/C ratios seemed to indicate that a sizable fraction of marine DOM molecules with large O/C ratios were simply not getting ionized under the employed experimental conditions. Hence, ion suppres-

10 sion was a decisive factor in influencing FTICR mass spectra of the complex marine DOM fractions. Mass spectrometry derived elemental C/N ratios were growing from 18.4 (sample FISH) to 24.1 (sample 5446 m), indicative of slight preference to ionize N-containing molecules over others, however with declining discrimination (cf. Table 1). This divergence indicated again variable chemical environments for CHO and CHNO

15 molecules at different water depths. The MS-derived C/S atomic ratios near continually increased from surface to deep DOM (Table 5), indicating progressive depletion of sulfur, in line with element analyses (Fig. 17).

3.13 The role of metal coordination compounds in the transverse and longitudinal NMR relaxation of marine DOM

20 Isolation of marine DOM by means of solid phase extraction (SPE) imposes less severe chemical alterations than the IHSS based extraction protocol (International Humic Substances Society). Nevertheless, SPE of marine waters includes an acidification step down to pH ~2. Here, metal ions with lesser binding constants to organic matter will be preferentially released from marine DOM during SPE extraction and replaced

25 with protons (Sohrin et al., 2008). Hence, the metals identified in isolated DOM will not reflect the authentic marine DOM metal composition as found in the ocean (Pohl et al., 2011; Sohrin et al., 2008; Vraspir and Butler, 2009). In addition, isolation of marine DOM was performed via standard glass bottles without specific care given to metal

content (affecting, e.g. the quality of Al, B, Na, Si and trace metal analyses). However, large sampling volumes (>50 l of seawater) and concentration factors (Table 1) as well as uniform work-up designed to result in sufficient isolated DOM for high quality NMR analyses enabled sensitive metal analyses, too. Hence, determination of metal concentration in SPE-derived DOM clarified the potential contributions of metal ions to the observed acceleration of transverse NMR relaxation with increasing water depth which could be twofold. Coordination of DOM ligands to metal ions will likely reduce molecular mobility of the organic ligands, whereas complexation of DOM with paramagnetic metal ions (like e.g. $Fe^{2/3+}$, Mn^{2+}, $Cu^{+/2+}$) will transfer electron spin density to ligand atoms, which often causes "bleaching" of NMR resonances (Smernik and Oades, 2002; Turano et al., 2010; Bertini et al., 2008; Kleckner and Foster, 2011).

No uniform trends of metal content from surface to deep marine DOM were identified in the four marine DOM samples: some metals were found with a near uniform distribution throughout the DOM samples whereas others were enriched at depth (Fig. 17; Supporting Online Table 3). Metals associated with life functions (micronutrients for organisms such as e.g.: Ca, Co, Cu, Fe, K, Mg, Mn, Mo, P, V, Zn) have commonly not been found enriched in the two surface DOM (FISH and FMAX) which supposedly reflect enhanced proportions of biological activity. Otherwise, thorium, phosphorus and sulfur declined from surface to depth in line with common distribution in marine DOM. Phosphorus and sulfur attached to DOM in the form of phosphate and sulfate would increase molecular weight and size, and perhaps attenuate molecular mobility, without clear ^{1}H and ^{13}C NMR signature in the complex DOM mixture. Near uniform distribution throughout all DOM samples was found for Al, As, Cr, Mo, Sr and Zn. The considerable deviation of the metal/DOM ratio in comparison with common oceanic metal distribution at various water depths probably indicated variance in metal speciation in the different DOM, which could have been either related to chemical specificity and/or molecular size selectivity (Pohl et al., 2011; Takeda et al., 2009). Indications for any substantial leaching of metal ions from the bottom sediment were absent; the marginally increased metal concentrations at the bottom DOM (5446 m) found for the

ions of Ca, Cd, Mg and Zn were considered insignificant in this respect.

In the context of NMR relaxation, the most important ion to assess NMR behaviour was iron (Fe), a paramagnetic and strongly complexing metal (Witter et al., 2000) for which a large contribution for accelerating transverse NMR relaxation could be expected. Remarkably, Fe was found notably enriched in surface DOM sample FISH, which nevertheless displayed well resolved NMR spectra (e.g. COSY, cf. Fig. 7, Supporting Online Fig. 4). Other paramagnetic 3d metals, like V, Cr, Mn, Co and Ni as well as Cu were more uniformly distributed and much less abundant than Fe; the abundance of Ni, the second most abundant metal of this series also declined significantly from surface to deep DOM (Fig. 17, Supporting Online Table 3). Hence, the acceleration of transverse NMR relaxation from surface to deep DOM was not primarily caused by metal content of DOM.

4 Conclusions

Marine DOM was investigated by high-resolution organic structural spectroscopy which provided unprecedented molecular level detail of complex unknowns. NMR spectroscopy (provides isotope-specific atomic short range order) and FTICR mass spectrometry (provides molecular mass of ions) are the only two methods in the analysis of extremely intricate organic mixtures like marine DOM in which the measured response *directly* relates to molecular parameters. Any other method to characterize polydisperse materials has to rely on transfer functions of mainly unknown shape and amplitude.

Marine DOM isolated by means of solid phase extraction (SPE) possessed characteristics of sufficiently slow transverse NMR relaxation to allow for the acquisition of 2-D NMR spectra with excellent cross peak resolution. The sensitivity and resolution gain available in high field NMR spectra has enabled unprecedented NMR signal attribution in marine DOM, which in contrast to classical degradative target analysis covered a major fraction of carbon. In fact, NMR is the most potent non-target discovery

tool which solely discriminates on the basis of differential longitudinal and transverse NMR relaxation which barely affected one-dimensional proton and carbon NMR spectra of marine DOM. The intrinsic resolution of complementary multi-dimensional NMR spectroscopy compared favourably with the intricacy of marine DOM and allowed the depiction of significant individual molecular oceanic DOM signatures to elucidate the respective holistic memories of oceanic biogeochemical history.

Complementary homonuclear 2-D NMR spectra with high sensitivity and appreciable resolution allowed to trace and quantify organic molecular diversity: JRES NMR spectra as screening and confirmation tools for abundant biogeochemical signatures and COSY NMR spectra with superior cross peak resolution to simultaneously discriminate hundreds of molecules, at least in biologically productive marine waters in which abundant molecular diversity of presumptive biological origin prevails. Alternatively, cumulative superposition of faint HSQC and TOCSY cross peaks with extended areas of chemical shift allowed for a far reaching structural assessment of sp^2-hybridized carbon chemical environments in marine DOM. By combining ^{1}H, ^{13}C and HSQC NMR spectra, olefinic unsaturation was found more prevalent in marine DOM than aromatic unsaturation. Olefins, of which the largest proportion is probably of ultimately biological origin will be much better traceable and connected with ultimate precursors and defined biogeochemical alteration mechanisms than aromatic geochemical materials like aromatic thermogenic organic carbon which (TMOC) originated from less specific sources and precursors and has been aged beyond other diagenetic timescales.

Future non-target molecular DOM characterization by means of NMR and FTICR mass spectrometry will employ full scale NMR characterization of intact marine DOM in conjunction with fractionation to further resolve this intricate mixture (Gaspar et al., 2010). Then, FTICR mass spectra will suffer less from intrinsic averaging because lesser numbers of isomeric molecules will be projected onto individual mass peaks. Individual adjustment of NMR acquisition parameters for DOM fractions and comparison of standardized NMR measurements with educated data base search (Woods et al., 2011) will enable the resolution, identification and quantification of hundreds to

eventually several thousands of individual marine DOM molecules. Finally, the faithful depiction of marine DOM organic complexity will enable a clear perception of oceanic contributions to the global carbon and other element cycles.

Supplementary material related to this article is available online at: http://www.biogeosciences-discuss.net/9/745/2012/bgd-9-745-2012-supplement. pdf.

References

Aihara, J. I., Sekine, R., and Ishida, T.: Electronic and magnetic characteristics of polycyclic aromatic hydrocarbons with factorizable Kekulé structure counts, J. Phys. Chem. A, 115, 9314–9321, 2011.

Aluwihare, L. I., Repeta, D. J., and Chen, R. F.: Chemical composition and cycling of dissolved organic matter in the mid-atlantic bight, Deep-Sea Res., Part II: Topical Studies in Oceanography, 49, 4421–4437, 2002.

Amrani, A., Turner, J. W., Ma, Q. S., Tang, Y. C., and Hatcher, P. G.: Formation of sulfur and nitrogen cross-linked macromolecules under aqueous conditions, Geochim. Cosmochim. Ac., 71, 4141–4160, 2007.

Andreae, M. O. and Crutzen, P. J.: Atmospheric aerosols: Biogeochemical sources and role in atmospheric chemistry, Science, 276, 1052–1058, 1997.

Bakhmutov, V. I.: Practical NMR Relaxation for Chemists, John Wiley & Sons, Chichester, England, 2004.

Battin, T. J., Luyssaert, S., Kaplan, L. A., Aufdenkampe, A. K., Richter, A., and Tranvik, L. J.: The boundless carbon cycle, Nature Geoscience, 2, 598–600, 2009.

Bauschlicher, C. W., Peeters, E., and Allamandola, L. J.: The infrared spectra of very large irregular polycyclic aromatic hydrocarbons (PAHs): Observational probes of astronomical pah geometry, size, and charge, Astrophys. J., 697, 311–327, 2009.

Benner, R.: Chemical composition and reactivity, in: Biogeochemistry of marine dissolved organic matter, edited by: Hansell, D. A. and Carlson, C. A., Academic Press, 59–90, 2002.

Bertini, I., Luchinat, C., Parigi, G., and Pierattelli, R.: Perspectives in paramagnetic NMR of metalloproteins, Dalton T, 3782–3790, 2008.

Blunt, J. W., Copp, B. R., Munro, M. H. G., Northcote, P. T., and Prinsep, M. R.: Marine natural products, Nat. Prod. Rep., 27, 165–237, 2010.

Buddrus, J., Burba, P., Lambert, J., and Herzog, H.: Quantification of partial structures of aquatic humic substances by one- and two-dimensional solution ^{13}C nuclear magnetic resonance spectroscopy, Anal. Chem., 61, 628–631, 1989.

Cane, D. E. and Ikeda, H.: Exploration and mining of the bacterial terpenome, Acc. Chem. Res., 39, doi:10.1021/ar200198d, 2011.

Carper, W. R., Wahlbeck, P. G., and Dolle, A.: C-13 NMR relaxation rates: Separation of dipolar and chemical shift anisotropy effects, J. Phys. Chem. A, 108, 6096–6099, 2004.

Case, D. A.: The use of chemical shifts and their anisotropies in biomolecular structure determination, Curr. Opin. Struc. Biol., 8, 624–630, 1998.

Cavanagh, J., Fairbrother, W. J., Palmer III, A. G., Rance, M., and Skelton, N. J.: Protein NMR Spectroscopy, Elsevier, Burlington, USA, 2007.

Cheng, C. H., Lehmann, J., Thies, J. E., Burton, S. D., and Engelhard, M. H.: Oxidation of black carbon by biotic and abiotic processes, Org. Geochem., 37, 1477–1488, 2006.

Cho, Y., Kim, Y. H., and Kim, S.: Planar limit-assisted structural interpretation of saturates/aromatics/resins/asphaltenes fractionated crude oil compounds observed by fourier transform ion cyclotron resonance mass spectrometry, Anal. Chem., 83, 6068–6073, 2011.

Coble, P. G.: Marine optical biogeochemistry: The chemistry of ocean color, Chem. Rev., 107, 402–418, 2007.

Cook, R. L., Langford, C. H., Yamdagni, R., and Preston, C. M.: A modified cross-polarization magic angle spinning ^{13}C NMR procedure for the study of humic materials, Anal. Chem., 68, 3979–3986, 1996.

Crouch, R. C., Llanos, W., Mehr, K. G., Hadden, C. E., Russell, D. J., and Martin, G. E.:

Title Page

Abstract	Introduction
Conclusions	References
Tables	Figures

◄ | ►◄

◄ | ►

Back | Close

Full Screen / Esc

Printer-friendly Version

Interactive Discussion

Applications of cryogenic NMR probe technology to long-range ^{1}H-^{15}N 2D NMR studies at natural abundance, Magn. Reson. Chem., 39, 555–558, 2001.

Dickens, A. F., Gelinas, Y., Masiello, C. A., Wakeham, S., and Hedges, J. I.: Reburial of fossil organic carbon in marine sediments, Nature, 427, 336–339, 2004.

Dittmar, T. and Kattner, G.: Recalcitrant dissolved organic matter in the ocean: Major contribution of small amphiphilics, Mar. Chem., 82, 115–123, 2003a.

Dittmar, T. and Kattner, G.: The biogeochemistry of the river and shelf ecosystem of the arctic ocean: A review, Mar. Chem., 83, 103–120, 2003b.

Dittmar, T. and Koch, B. P.: Thermogenic organic matter dissolved in the abyssal ocean, Mar. Chem., 102, 208–217, 2006.

Dittmar, T. and Paeng, J.: A heat-induced molecular signature in marine dissolved organic matter, Nature Geoscience, 2, 175–179, 2009.

Dittmar, T., Koch, B., Hertkorn, N., and Kattner, G.: A simple and efficient method for the solid-phase extraction of dissolved organic matter (SPE-DOM) from seawater, Limnol. Oceanogr.-Meth., 6, 230–235, 2008.

Effemey, M., Lang, J., and Kowalewski, J.: Multiple-field carbon-13 and proton relaxation in sucrose in viscous solution, Magn. Reson. Chem., 38, 1012–1018, 2000.

Einsiedl, F., Hertkorn, N., Wolf, M., Frommberger, M., Schmitt-Kopplin, P., and Koch, B. P.: Rapid biotic molecular transformation of fulvic acids in a karst aquifer, Geochim. Cosmochim. Ac., 71, 5474–5482, 2007.

Falco, C., Caballero, F. P., Babonneau, F., Gervais, C., Laurent, G., Titirici, M.-M., and Baccile, N.: Hydrothermal Carbon from Biomass: Structural Differences between Hydrothermal and Pyrolyzed Carbons via Solid State NMR, Langmuir, 27, 14460–14471, 2011.

Flerus, R., Koch, B. P., Lechtenfeld, O. J., McCallister, S. L., Schmitt-Kopplin, P., Benner, R., Kaiser, K., and Kattner, G.: A molecular perspective on the ageing of marine dissolved organic matter, Biogeosciences Discuss., 8, 11453–11488, doi:10.5194/bgd-8-11453-2011, 2011a.

Flerus, R., Koch, B. P., Schmitt-Kopplin, P., Witt, M., and Kattner, G.: Molecular level investigation of reactions between dissolved organic matter and extraction solvents using FT-ICR MS, Mar. Chem., 124, 100–107, 2011b.

Gaspar, A., Harir, M., Hertkorn, N., and Schmitt-Kopplin, P.: Preparative free-flow electrophoretic offline ESI-Fourier transform ion cyclotron resonance/MS analysis of Suwannee River fulvic acid, Electrophoresis, 31, 2070–2079, 2010.

Graeve, M. and Janssen, D.: Improved separation and quantification of neutral and polar lipid classes by HPLC-ELSD using a monolithic silica phase: Application to exceptional marine lipids, J. Chromatogr. B, 877, 1815–1819, 2009.

Hansell, D. A. and Carlson, C. A.: Deep-ocean gradients in the concentration of dissolved organic carbon, Nature, 395, 263–266, 1998.

Hansen, P. E.: ^{13}C NMR of Polycyclic Aromatic Compounds. A Review, Org. Magn. Reson., 12, 109–142, 1979.

Hansen, A. L. and Al-Hashimi, H. M.: Dynamics of large elongated RNA by NMR carbon relaxation, J. Am. Chem. Soc., 129, 16072–16082, 2007.

Hedges, J. I. and Oades, J. M.: Comparative organic geochemistries of soils and marine sediments, Org. Geochem., 27, 319–361, 1997.

Hedges, J. I., Baldock, J. A., Gelinas, Y., Lee, C., Peterson, M., and Wakeham, S. G.: Evidence for non-selective preservation of organic matter in sinking marine particles, Nature, 409, 801–804, 2001.

Hedges, J. I., Baldock, J. A., Gelinas, Y., Lee, C., Peterson, M. L., and Wakeham, S. G.: The biochemical and elemental compositions of marine plankton: A NMR perspective, Mar. Chem., 78, 47–63, 2002.

Hernes, P. J. and Benner, R.: Terrigenous organic matter sources and reactivity in the North Atlantic Ocean and a comparison to the Arctic and Pacific Oceans, Mar. Chem., 100, 66–79, 2006.

Hertkorn, N. and Kettrup, A.: Molecular level structural analysis of natural organic matter and of humic substances by multinuclear and higher dimensional NMR spectroscopy in: Use of humic substances to remediate polluted environments: From theory to practice, edited by: Perminova, I., Hatfield, K., and Hertkorn, N., Springer Netherlands, 391–435, 2005.

Hertkorn, N., Günzl, A., Freitag, D., and Kettrup, A.: Nuclear Magnetic Resonance Spectroscopy Investigations of Silylated Refractory Organic Substances, in: Refractory Organic Substances in the Environment (DFG-Schwerpunktsprogramm Refraktäre Organische Säuren in Gewässern), edited by: Frimmel, F. H. and Abbt-Braun, G., Wiley-VCH, p. 129–145, 2002a.

Hertkorn, N., Permin, A., Perminova, I., Kovalevskii, D., Yudov, M., Petrosyan, V., and Kettrup, A.: Comparative analysis of partial structures of a peat humic and fulvic acid using one- and two-dimensional nuclear magnetic resonance spectroscopy, J. Environ. Qual., 31, 375–387, 2002b.

Title Page

Abstract | Introduction

Conclusions | References

Tables | Figures

◄ | ►

◄ | ►

Back | Close

Full Screen / Esc

Printer-friendly Version

Interactive Discussion

Hertkorn, N., Perdue, E. M., and Kettrup, A.: A potentiometric and [113]Cd nmr study of cadmium complexation by natural organic matter at two different magnetic field strengths, Anal. Chem., 76, 6327–6341, 2004.

Hertkorn, N., Benner, R., Frommberger, M., Schmitt-Kopplin, P., Witt, M., Kaiser, K., Kettrup, A., and Hedges, J. I.: Characterization of a major refractory component of marine dissolved organic matter, Geochim. Cosmochim. Ac., 70, 2990–3010, 2006.

Hertkorn, N., Ruecker, C., Meringer, M., Gugisch, R., Frommberger, M., Perdue, E. M., Witt, M., and Schmitt-Kopplin, P.: High-precision frequency measurements: Indispensable tools at the core of the molecular-level analysis of complex systems, Analytical and Bioanalytical Chemistry, 389, 1311–1327, 2007.

Hertkorn, N., Frommberger, M., Witt, M., Koch, B. P., Schmitt-Kopplin, P., and Perdue, E. M.: Natural organic matter and the event horizon of mass spectrometry, Anal. Chem., 80, 8908–8919, 2008.

Hoch, J. C. and Stern, A. S.: NMR Data Processing, John Wiley & Sons, Wiley-Liss, New York, USA, 1996.

Hockaday, W. C., Grannas, A. M., Kim, S., and Hatcher, P. G.: Direct molecular evidence for the degradation and mobility of black carbon in soils from ultrahigh-resolution mass spectral analysis of dissolved organic matter from a fire-impacted forest soil, Org. Geochem., 37, 501–510, 2006.

Hopkinson, C. S. and Vallino, J. J.: Efficient export of carbon to the deep ocean through dissolved organic matter, Nature, 433, 142–145, 2005.

Jiao, N., Herndl, G. J., Hansell, D. A., Benner, R., Kattner, G., Wilhelm, S. W., Kirchman, D. L., Weinbauer, M. G., Luo, T. W., Chen, F., and Azam, F.: Microbial production of recalcitrant dissolved organic matter: Long-term carbon storage in the global ocean, Nat. Rev. Microbiol., 8, 593–599, 2010.

Jimenez, J. L., Canagaratna, M. R., Donahue, N. M., Prevot, A. S. H., Zhang, Q., Kroll, J. H., DeCarlo, P. F., Allan, J. D., Coe, H., Ng, N. L., Aiken, A. C., Docherty, K. S., Ulbrich, I. M., Grieshop, A. P., Robinson, A. L., Duplissy, J., Smith, J. D., Wilson, K. R., Lanz, V. A., Hueglin, C., Sun, Y. L., Tian, J., Laaksonen, A., Raatikainen, T., Rautiainen, J., Vaattovaara, P., Ehn, M., Kulmala, M., Tomlinson, J. M., Collins, D. R., Cubison, M. J., Dunlea, E. J., Huffman, J. A., Onasch, T. B., Alfarra, M. R., Williams, P. I., Bower, K., Kondo, Y., Schneider, J., Drewnick, F., Borrmann, S., Weimer, S., Demerjian, K., Salcedo, D., Cottrell, L., Griffin, R., Takami, A., Miyoshi, T., Hatakeyama, S., Shimono, A., Sun, J. Y., Zhang, Y. M., Dzepina, K., Kimmel, J.

R., Sueper, D., Jayne, J. T., Herndon, S. C., Trimborn, A. M., Williams, L. R., Wood, E. C., Middlebrook, A. M., Kolb, C. E., Baltensperger, U., and Worsnop, D. R.: Evolution of organic aerosols in the atmosphere, Science, 326, 1525–1529, 2009.

Kaiser, E., Simpson, A. J., Dria, K. J., Sulzberger, B., and Hatcher, P. G.: Solid-state and multidimensional solution-state NMR of solid phase extracted and ultrafiltered riverine dissolved organic matter, Environ. Sci. Technol., 37, 2929–2935, 2003.

Kelleher, B. P. and Simpson, A. J.: Humic substances in soils: Are they really chemically distinct?, Environ. Sci. Technol., 40, 4605–4611, 2006.

Kleckner, I. R. and Foster, M. P.: An introduction to NMR-based approaches for measuring protein dynamics, BBA-Proteins Proteom., 1814, 942–968, 2011.

Koch, B. P. and Dittmar, T.: From mass to structure: An aromaticity index for high-resolution mass data of natural organic matter, Rapid Commun. Mass Sp., 20, 926–932, 2006.

Koch, B. P., Witt, M. R., Engbrodt, R., Dittmar, T., and Kattner, G.: Molecular formulae of marine and terrigenous dissolved organic matter detected by electrospray ionization fourier transform ion cyclotron resonance mass spectrometry, Geochim. Cosmochim. Ac., 69, 3299–3308, 2005.

Koch, B. P., Kattner, G., and Herndl, G. I.: Sources and rapid biogeochemical transformation of dissolved organic matter in the atlantic surface ocean, Biogeosciences Discuss., in preparation, 2011.

Koprivnjak, J. F., Pfromm, P. H., Ingall, E., Vetter, T. A., Schmitt-Kopplin, P., Hertkorn, N., Frommberger, M., Knicker, H., and Perdue, E. M.: Chemical and spectroscopic characterization of marine dissolved organic matter isolated using coupled reverse osmosiselectrodialysis, Geochim. Cosmochim. Ac., 73, 4215–4231, 2009.

Korzhnev, D. M., Kloiber, K., and Kay, L. E.: Multiple-quantum relaxation dispersion NMR spectroscopy probing millisecond time-scale dynamics in proteins: Theory and application, J. Am. Chem. Soc., 126, 7320–7329, 2004a.

Korzhnev, D. M., Salvatella, X., Vendruscolo, M., Di Nardo, A. A., Davidson, A. R., Dobson, C. M., and Kay, L. E.: Low-populated folding intermediates of Fyn SH3 characterized by relaxation dispersion NMR, Nature, 430, 586–590, 2004b.

Kovacs, H., Moskau, D., and Spraul, M.: Cryogenically cooled probes – a leap in NMR technology, Prog. Nucl. Mag. Res. Sp., 46, 131–155, 2005.

Kovalevskii, D. V., Permin, A. B., Perminova, I. V., and Petrosyan, V. S.: Recovery of conditions for quantitative measuring the NMR spectra of humic acids, Vestn. Mosk. U. Khim., 41, 39–

42, 2000.

Kroll, J. H., Donahue, N. M., Jimenez, J. L., Kessler, S. H., Canagaratna, M. R., Wilson, K. R., Altieri, K. E., Mazzoleni, L. R., Wozniak, A. S., Bluhm, H., Mysak, E. R., Smith, J. D., Kolb, C. E., and Worsnop, D. R.: Carbon oxidation state as a metric for describing the chemistry of atmospheric organic aerosol, Nat. Chem., 3, 133–139, 2011.

Kujawinski, E. B.: Electrospray ionization fourier transform ion cyclotron resonance mass spectrometry (ESI FT-ICR MS): Characterization of complex environmental mixtures, Environ. Forensics, 3, 207–216, 2002.

Kujawinski, E. B., Longnecker, K., Blough, N. V., Del Vecchio, R., Finlay, L., Kitner, J. B., and Giovannoni, S. J.: Identification of possible source markers in marine dissolved organic matter using ultrahigh resolution mass spectrometry, Geochim. Cosmochim. Ac., 73, 4384–4399, 2009.

Lam, B., Baer, A., Alaee, M., Lefebvre, B., Moser, A., Williams, A., and Simpson, A. J.: Major structural components in freshwater dissolved organic matter, Environ. Sci. Technol., 41, 8240–8247, 2007.

Leenheer, J. A., Nanny, M. A., and McIntyre, C.: Terpenoids as major precursors of dissolved organic matter in landfill leachates, surface water, and groundwater, Environ. Sci. Technol., 37, 2323–2331, 2003.

Lipp, J. S. and Hinrichs, K. U.: Structural diversity and fate of intact polar lipids in marine sediments, Geochim. Cosmochim. Ac., 73, 6816–6833, 2009.

Mahieu, N., Powlson, D. S., and Randall, E. W.: Statistical analysis of published carbon-13 CPMAS NMR spectra of soil organic matter, Soil Sci. Soc. Am. J., 63, 307–319, 1999.

Maie, N., Parish, K. J., Watanabe, A., Knicker, H., Benner, R., Abe, T., Kaiser, K., and Jaffe, R.: Chemical characteristics of dissolved organic nitrogen in an oligotrophic subtropical coastal ecosystem, Geochim. Cosmochim. Ac., 70, 4491–4506, 2006.

Martin, G. E., Hilton, B. D., Moskau, D., Freytag, N., Kessler, K., and Colson, K.: Long-range [1]H-^{15}N heteronuclear shift correlation across wide F1 spectral windows, Magn. Reson. Chem., 48, 935–937, 2010.

Masiello, C. A.: New directions in black carbon organic geochemistry, Mar. Chem., 92, 201–213, 2004.

Masiello, C. A. and Druffel, E. R. M.: Black carbon in deep-sea sediments, Science, 280, 1911–1913, 1998.

McCaul, M. V., Sutton, D., Simpson, A. J., Spence, A., McNally, D. J., Moran, B. W., Goel, A.,

Title Page

Abstract | Introduction

Conclusions | References

Tables | Figures

|◄ | ►|

◄ | ►

Back | Close

Full Screen / Esc

Printer-friendly Version

Interactive Discussion

O'Connor, B., Hart, K., and Kelleher, B. P.: Composition of dissolved organic matter within a lacustrine environment, Environ. Chem., 8, 146–154, 2011.

McKee, G. A. and Hatcher, P. G.: Alkyl amides in two organic-rich anoxic sediments: A possible new abiotic route for N sequestration, Geochim. Cosmochim. Ac., 74, 6436–6450, 2010.

Mopper, K., Stubbins, A., Ritchie, J. D., Bialk, H. M., and Hatcher, P. G.: Advanced instrumental approaches for characterization of marine dissolved organic matter: Extraction techniques, mass spectrometry, and nuclear magnetic resonance spectroscopy, Chem. Rev., 107, 419–442, 2007.

Moskau, D.: Application of real time digital filters in NMR spectroscopy, Concept Magnetic Res., 15, 164–176, 2002.

Mulder, F. A. A. and Akke, M.: Carbonyl ^{13}C transverse relaxation measurements to sample protein backbone dynamics, Magn. Reson. Chem., 41, 853–865, 2003.

Neudecker, P., Lundstrom, P., and Kay, L. E.: Relaxation dispersion NMR spectroscopy as a tool for detailed studies of protein folding, Biophys. J., 96, 2045–2054, 2009.

Ohno, T., He, Z. Q., Sleighter, R. L., Honeycutt, C. W., and Hatcher, P. G.: Ultrahigh resolution mass spectrometry and indicator species analysis to identify marker components of soil- and plant biomass-derived organic matter fractions, Environ. Sci. Technol., 44, 8594–8600, 2010.

Panagiotopoulos, C., Repeta, D. J., and Johnson, C. G.: Characterization of methyl sugars, 3-deoxysugars and methyl deoxysugars in marine high molecular weight dissolved organic matter, Org. Geochem., 38, 884–896, 2007.

Paytan, A., Mackey, K. R. M., Chen, Y., Lima, I. D., Doney, S. C., Mahowald, N., Labiosa, R., and Post, A. F.: Toxicity of atmospheric aerosols on marine phytoplankton, P. Natl. Acad. Sci. USA, 106, 4601–4605, 2009.

Perdue, E. M., Hertkorn, N., and Kettrup, A.: Substitution patterns in aromatic rings by increment analysis. Model development and application to natural organic matter, Anal. Chem., 79, 1010–1021, 2007.

Pohl, C., Croot, P. L., Hennings, U., Daberkow, T., Budeus, G., and v. d. Loeff, M. R.: Synoptic transects on the distribution of trace elements (Hg, Pb, Cd, Cu, Ni, Zn, Co, Mn, Fe, and Al) in surface waters of the Northern- and Southern East Atlantic, J. Marine Syst., 84, 28–41, 2011.

Pos, W. H., Riemer, D. D., and Zika, R. G.: Carbonyl sulfide (OCS) and carbon monoxide (CO) in natural waters: Evidence of a coupled production pathway, Mar. Chem., 62, 89–101,

1998.

Repeta, D. J., Quan, T. M., Aluwihare, L. I., and Accardi, A. M.: Chemical characterization of high molecular weight dissolved organic matter in fresh and marine waters, Geochim. Cosmochim. Ac., 66, 955–962, 2002.

5 Rezende, C. E., Pfeiffer, W. C., Martinelli, L. A., Tsamakis, E., Hedges, J. I., and Keil, R. G.: Lignin phenols used to infer organic matter sources to Sepetiba Bay – RJ, Brasil, Estuar. Coast. Shelf S., 87, 479–486, 2010.

Ritchie, J. D. and Perdue, E. M.: Analytical constraints on acidic functional groups in humic substances, Org. Geochem., 39, 783–799, 2008.

10 Schmidt, F., Koch, B. P., Elvert, M., Schmidt, G., Witt, M., and Hinrichs, K. U.: Diagenetic transformation of dissolved organic nitrogen compounds under contrasting sedimentary redox conditions in the black sea, Environ. Sci. Technol., 45, 5223–5229, 2011.

Schmitt-Kopplin, P., Hertkorn, N., Schulten, H. R., and Kettrup, A.: Structural changes in a dissolved soil humic acid during photochemical degradation processes under O_2 and N_2

15 atmosphere, Environ. Sci. Technol., 32, 2531–2541, 1998.

Schmitt-Kopplin, P., Gabelica, Z., Gougeon, R. D., Fekete, A., Kanawati, B., Harir, M., Gebefuegi, I., Eckel, G., and Hertkorn, N.: High molecular diversity of extraterrestrial organic matter in murchison meteorite revealed 40 years after its fall, P. Natl. Acad. Sci. USA, 107, 2763–2768, 2010a.

20 Schmitt-Kopplin, P., Gelencser, A., Dabek-Zlotorzynska, E., Kiss, G., Hertkorn, N., Harir, M., Hong, Y., and Gebefuegi, I.: Analysis of the unresolved organic fraction in atmospheric aerosols with ultrahigh-resolution mass spectrometry and nuclear magnetic resonance spectroscopy: Organosulfates as photochemical smog constituents, Anal. Chem., 82, 8017–8026, 2010b.

25 Simpson, A. J. and Brown, S. A.: Purge NMR: Effective and easy solvent suppression, J. Magn. Reson., 175, 340–346, 2005.

Simpson, A. J., Kingery, W. L., Hayes, M. H. B., Spraul, M., Humpfer, E., Dvortsak, P., Kerssebaum, R., Godejohann, M., and Hofmann, M.: Molecular structures and associations of humic substances in the terrestrial environment, Naturwissenschaften, 89, 84–88, 2002.

30 Simpson, A. J., Kingery, W. L., and Hatcher, P. G.: The identification of plant derived structures in humic materials using three-dimensional NMR spectroscopy, Environ. Sci. Technol., 37, 337–342, 2003.

Simpson, A. J., McNally, D. J., and Simpson, M. J.: NMR spectroscopy in environmental re-

search: From molecular interactions to global processes, Prog. Nucl. Mag. Res. Sp., 58, 97–175, 2011.

Smernik, R. J. and Oades, J. M.: Effects of added paramagnetic ions on the ^{13}C CP MAS NMR spectrum of a de-ashed soil, Geoderma, 89, 219–248, 1999.

Smernik, R. J. and Oades, J. M.: Effect of paramagnetic cations on solid state ^{13}C nuclear magnetic resonance spectra of natural organic materials, Commun. Soil Sci. Plan., 31, 3011–3026, 2000.

Smernik, R. J. and Oades, J. M.: Paramagnetic effects on solid state carbon-13 nuclear magnetic resonance spectra of soil organic matter, J. Environ. Qual., 31, 414–420, 2002.

Sohrin, Y., Urushihara, S., Nakatsuka, S., Kono, T., Higo, E., Minami, T., Norisuye, K., and Umetani, S.: Multielemental determination of GEOTRACES Key trace metals in seawater by ICPMS after preconcentration using an ethylenediaminetriacid chelating resin, Anal. Chem., 80, 6267–6273, 2008.

Spencer, R. G.: Equivalence of the time-domain matched filter and the spectral-domain matched filter in one-dimensional NMR spectroscopy, Concept Magn. Reson. A, 36A, 255–265, 2010.

Stenson, A. C., Marshall, A. G., and Cooper, W. T.: Exact masses and chemical formulas of individual Suwannee River fulvic acids from ultrahigh resolution electrospray ionization Fourier transform ion cyclotron resonance mass spectra, Anal. Chem., 75, 1275–1284, 2003.

Takeda, A., Tsukada, H., Takaku, Y., and Hisamatsu, S.: Fractionation of metal complexes with dissolved organic matter in a rhizosphere soil solution of a humus-rich andosol using size exclusion chromatography with inductively coupled plasma-mass spectrometry, Soil Sci. Plant Nutr., 55, 349–357, 2009.

Tomczak, M. and Godfrey, J. S.: Regional Oceanography: An Introduction, 2nd ed., Daya Publishing House, Delhi, 390 pp., 2003.

Tominaga, K., Sakamoto, Y., Fujimaki, Y., Takekawa, M., and Ohshima, S.: Structural analysis of hepta-, nona-, and undeca-cyclic aromatic hydrocarbons by NMR spectroscopy, Polycyclic Aromatic Compounds, 30, 274–286, 2010.

Traficante, D. D. and Rajabzadeh, M.: Optimum window function for sensitivity enhancement of NMR signals, Concept Magnetic Res., 12, 83–101, 2000.

Turano, P., Lalli, D., Felli, I. C., Theil, E. C., and Bertini, I.: NMR reveals pathway for ferric mineral precursors to the central cavity of ferritin, P. Natl. Acad. Sci. USA, 107, 545–550, 2010.

Title Page

Abstract | Introduction

Conclusions | References

Tables | Figures

◀◀ | ▶▶

◀ | ▶

Back | Close

Full Screen / Esc

Printer-friendly Version

Interactive Discussion

Vraspir, J. M. and Butler, A.: Chemistry of marine ligands and siderophores, Annu. Rev. Mar. Sci., 1, 43–63, 2009.

Walker, B. D., Beaupre, S. R., Guilderson, T. P., Druffel, E. R. M., and McCarthy, M. D.: Large-volume ultrafiltration for the study of radiocarbon signatures and size vs. age relationships in marine dissolved organic matter, Geochim. Cosmochim. Ac., 75, 5187–5202, 2011.

Witter, A. E., Hutchins, D. A., Butler, A., and Luther, G. W.: Determination of conditional stability constants and kinetic constants for strong model Fe-binding ligands in seawater, Mar. Chem., 69, 1–17, 2000.

Woods, G. C., Simpson, M. J., Koerner, P. J., Napoli, A., and Simpson, A. J.: HILIC-NMR: Toward the identification of individual molecular components in dissolved organic matter, Environ. Sci. Technol., 45, 3880–3886, 2011.

Xia, Y. L., Moran, S., Nikonowicz, E. P., and Gao, X. L.: Z-restored spin-echo ^{13}C 1D spectrum of straight baseline free of hump, dip and roll, Magn. Reson. Chem., 46, 432–435, 2008.

Ying, J. F., Grishaev, A. E., and Bax, A.: Carbon-13 chemical shift anisotropy in DNA bases from field dependence of solution NMR relaxation rates, Magn. Reson. Chem., 44, 302–310, 2006.

Zepp, R. G., Erickson, D. J., Paul, N. D., and Sulzberger, B.: Effects of solar UV radiation and climate change on biogeochemical cycling: Interactions and feedbacks, Photoch. Photobio. Sci., 10, 261–279, 2011.

Table 1. Details of marine DOM isolation and NMR sample preparation by PPL solid phase extraction; volume/weight ratios for methanolic extract were based on the methanol density at $20\,^{\circ}C = 0.7915\,\mathrm{g\,ml^{-1}}$.

Water depth	Marine water used for SPE	DOC of water [μM C]	DON of water [μM N]	C/N ratio of marine water	Original methanolic DOC solution obtained [g ml⁻¹]	Volumetric concentration factor from solid phase extraction SPE	C extraction yield carbon [μM C L⁻¹]	N extraction yield nitrogen [μM N l⁻¹]
5 m	50 l	71	4	16.7	38.1647/48.22	1037	27199 ± 71	1088 ± 27
48 m	50 l	76	5	14.7	71.57/90.42	553	20151 ± 741	816 ± 50
200 m	50 l	63	11	5.8	68.8024/86.93	575	18579 ± 0	723 ± 1
5446 m	50 l	47	5	9.2	39.3714/49.74	1005	14408 ± 377	533 ± 4

C/N ratio extract	Extraction yield carbon [%]	Extraction yield nitrogen [%]	Original CD₃OD solution used for NMR [g]	Dry matter of DOC used for NMR [mg]	CD₃OD used to dissolve DOC for NMR [mg]	Total computed DOC dry matter for extract [mg]
25.0 ± 0.7	37	24.8	23.4848	21.9	104.7	35.6
24.7 ± 2.4	44	28.3	34.2254	36.2	190.0	75.7
25.7 ± 0.1	40	11.3	30.7164	33.9	153.9	75.9
27.0 ± 0.9	43	10.2	16.6094	9.2	151.9	21.8

N. Hertkorn et al.

Table 2. Fundamental characteristics of key solution NMR experiments in the analysis of DOM (nominal bandwidth for ^{1}H NMR spectroscopy at B_0 = 18.8 T: 10 ppm × 800 Hz ppm^{-1} = 8000 Hz; ^{13}C NMR: 235 ppm × 200 Hz ppm^{-1} = 47 kHz nominal spectral width); * intrinsic nominal sensitivity refers to natural isotopic abundance (^{1}H: 99.985 %; ^{13}C: 1.1 %).

NMR experiment	nominal NMR matrix size [Hz^n] (apparent pixel/voxel resolution at B_0 = 18.8 T)	intrinsic nominal sensitivity* ($\gamma_{ex}\gamma_{det}^{3/2}$)	transfer mechanism and nominal time delay for magnetization transfer	F2/F1-apodization characteristics	general characteristics for the analysis of marine DOM
1-D ^{1}H	10 × 800 = 8 × 10^3	1	10 µs (spin echo delay)	exponential (resolution)	sensitive, quantitative, strong signal overlap
1-D ^{13}C	235 × 200 = 4.7 × 10^4	1.7 × 10^{-4}	10 µs (spin echo delay)	exponential (S/N ratio)	insensitive, informative, strong signal overlap
2-D ^{1}H,^{1}H JRES	8000 × 25 = 2 × 10^5	1	$^nJ_{HH}$ 100 ms	sine-bell (resolution)	good to reveal abundant molecular signatures; strong attenuation in case of fast transverse relaxation because of long duration of F1 increments
2-D ^{1}H,^{1}H COSY	8000^2 = 6.4 × 10^7	1	1/$^{2-3}J_{HH}$ 133 ms	sine-bell (resolution) and exponential/sine (S/N ratio and resolution)	discriminates in favour of molecular signatures; transfer amplitude ~1/J_{HH}; improved resolution of smaller couplings J_{HH} at higher number of F1 increments with attenuation from differential relaxation; cancellation of antiphase COSY cross peaks at higher linewidth is possible
2-D ^{1}H,^{1}H TOCSY	8000^2 = 6.4 × 10^7	1	1/2×$^{2-5}J_{HH}$ 100 ms	exponential/sine (both)	sensitive for detection of minor signatures; absorptive lineshape: contributions from small resonances are fairly visible; transfer amplitude ~1/2× J_{HH}
2-D ^{1}H,^{13}C HSQC family	8000 × 200^2 = 3.2 × 10^8	2.5 × 10^{-3}	1/$^1J_{CH}$ 3.5 ms	exponential/sine (both)	absorptive lineshape; good combination of sensitivity and large information content; spectral editing feasible
2-D ^{1}H,^{13}C HMBC	8000 × 200 × 235 = 3.8 × 10^8	2.5 × 10^{-3}	1/$^{2-4}J_{CH}$ 150 ms	exponential/sine (S/N ratio)	discriminates in favour of abundant molecular signatures because of low sensitivity; excellent peak dispersion; allows assembly of extended spin systems across heteroatoms and quaternary carbon
2-D ^{13}C,^{13}C INADEQUATE	47 000^2 = 2.3 × 10^9	3.1 × 10^{-6}	1/$^1J_{CC}$ 25 ms	exponential/sine (S/N ratio)	ultimate information about CC connectivities; not practical for marine NOM at present because of limited sensitivity
3-D ^{1}H,^{13}C,^{1}H HMQC-TOCSY	8000^2 × 200^2 = 2.6 × 10^{12}	2.5 × 10^{-3}	1/2×$^{2-5}J_{HH}$ + 1/$^1J_{CH}$: 100 ms	exponential/sine (S/N ratio)	excellent resolution with appreciable S/N ratio is now within realistic reach for high field NMR; in practice lesser utilizable resolution for ^{13}C (e.g. 1.7 × 10^7 volumetric pixels) (Simpson et al., 2003)

Table 3. ^{1}H NMR section integrals (percent of non-exchangeable protons) and key substructures from four marine DOM samples.

$\delta(^1$H) [ppm]	10–7.0	7.0–5.3	4.9–3.1	3.1–1.9	1.9–0.0	$H_{\text{olefinic}}/H_{\text{aromatic}}$	10–5.3 ($\underline{H}C_{sp^2}$)
Key substructures	$\underline{H}_{ar}$	$\underline{H}C{=}C$, $\underline{H}CO_2$	$\underline{H}CO$	$\underline{H}C$-N, $\underline{H}C$-C-X	$\underline{H}C$-C-C-		
FISH	1.82	4.56	22.20	28.97	42.45	2.50	6.38
FMAX	1.44	2.22	23.09	28.12	45.13	1.54	3.66
200	0.73	2.20	19.91	30.13	47.03	3.01	2.93
5446	1.59	1.91	19.61	30.55	46.34	1.20	3.50

Table 4. Top: ^{13}C NMR section integrals (percent of total carbon) and key substructures of marine DOM. Middle: Substructures used for NMR-derived reverse mixing model with nominal H/C and O/C rations given. Bottom: percentage of methine, methylene and methyl carbon related to total protonated ^{13}C NMR integral as derived from ^{13}C DEPT NMR spectra of marine DOM according to carbon multiplicity (left 3 columns) and relative proportions of these CH_n units binding to oxygen versus carbon chemical environments (nitrogen in the form of $N\text{-}CH_2$ and $N\text{-}CH_3$ is given if appropriate; cf. Fig. 9A and B).

$\delta(^{13}C)$ ppm	220–187	187–167	167–145	145–108	108–90	90–47	47–0	H/C ratio	O/C ratio
Key substructures	$\underline{C}{=}O$	$\underline{C}OX$	$\underline{C}_{ar}\text{-}O$	$\underline{C}_{ar}\text{-}C,H$	$O_2\underline{C}H$	$O\underline{C}H$	$C\underline{C}H$		
5 m	0.91	11.00	0.33	4.80	5.91	38.05	39.00	1.378	0.731
48 m	1.95	12.43	0.16	4.21	4.90	34.88	41.46	1.393	0.717
200 m	1.13	11.62	0.34	4.15	5.33	37.22	40.20	1.387	0.726
5446 m	2.15	13.34	1.16	3.41	4.73	34.61	40.60	1.373	0.741
NMR mixing model	C=O	COOH	$C_{ar}\text{-}O$	$C_{ar}\text{-}H$	O_2CH	OCH	CH_2		
H/C ratio	0	1	0	1	1	1	2		
O/C ratio	1	2	1	0	2	1	0		

DOM (depth)	CH total	CH$_2$ total	CH$_3$ total	ratio ($d_1/c_1/b_1/a_1$) H$\underline{C}_{ar}$-C/O-H$\underline{C}$-O/H$\underline{C}$-O/H$\underline{C}$-C	ratio (b_2/a_2) H$_2\underline{C}$-O/H$_2\underline{C}$-C	ratio (b_3/a_3) H$_3\underline{C}$-O/H$_3\underline{C}$-C
5 m	39	29	31	7.3/4.0/43.0/45.7	15/85	9/91
48 m	38	28	34	8.0/3.3/41.5/47.2	12/88	9/91
200 m	42	28	30	6.1/2.2/39.1/52.6	9/91	4/96
5446 m	35	39	26	8.1/2.3/32.9/56.7	3/97	5/95

Table 5. Counts of mass peaks as computed from negative electroscopy 12T FTICR mass spectra for singly charged ions with nitrogen rule check and 500 ppb tolerance.

Members of molecular series	FISH	FMAX	200 m	5446 m
CHO compounds	840 (24.6 %)	772 (24.6 %)	1167 (30.8 %)	1343 (39.3 %)
CHOS compounds	730 (21.4 %)	681 (21.7 %)	700 (18.5 %)	441 (12.9 %)
CHNO compounds	1054 (30.8 %)	976 (31.1 %)	1370 (36.1 %)	1391 (40.7 %)
CHNOS compounds	795 (23.3 %)	711 (22.6 %)	553 (14.6 %)	242 (7.1 %)
total	3419	3140	3790	3417
total number of mass peaks	7301	7244	7940	7537
average mass	367.60	366.18	372.07	381.75
percent of mass peaks attributed to CHO, CHOS, CHNO and CHNOS compositions	46.8 %	43.3 %	47.7 %	45.3 %
average H [%]	6.70	6.85	6.88	6.77
average C [%]	50.17	50.76	51.70	46.66
average O [%]	36.12	35.99	36.03	41.69
average N [%]	2.70	2.47	2.18	1.94
average S [%]	4.31	3.94	3.21	2.94
computed H/C ratio from FT-ICR mass peaks	1.60	1.62	1.60	1.74
computed O/C ratio from FT-ICR mass peaks	0.54	0.53	0.52	0.67
computed C/N ratio from FT-ICR mass peaks	18.44	20.55	23.72	24.05
computed C/S ratio from FT-ICR mass peaks	11.64	12.88	16.11	15.87
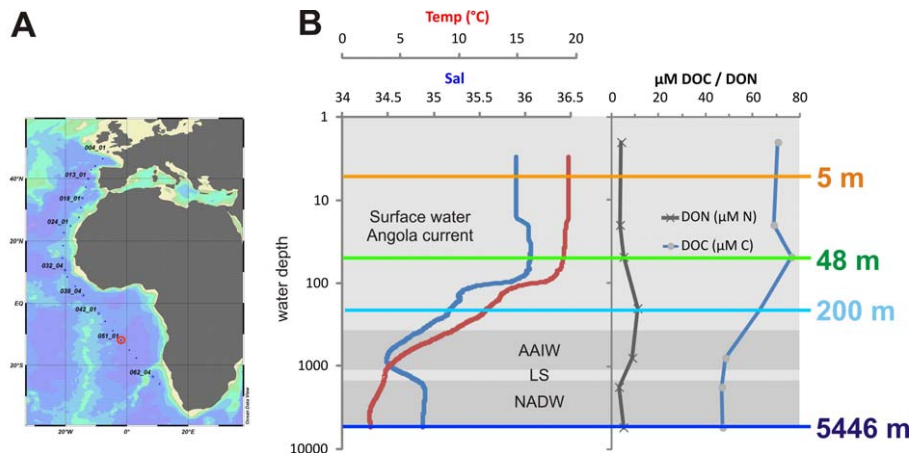
Fig. 1. (A) Sampling location of SPE-DOM during the R/V *Polarstern* cruise ANT XXV/1 on 27 November 2008 at 3.126° E; −17.737° S; figure by courtesy of G. Rohardt, AWI. **(B)** Conditions of oceanic waters; AAIW: Antarctic Intermediate Water (AAIW) which is derived from the Weddell Sea, Labrador Sea Water (LS) and North Atlantic Deep Water (NADW) which represents the oldest water mass in the profile (Tomczak and Godfrey, 2003); note logarithmic display of water depth for better resolution of sampling depths.
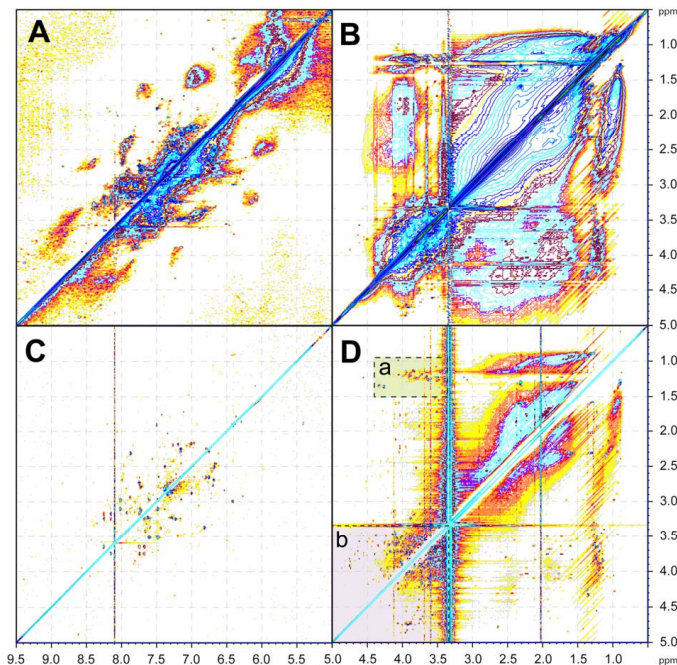
Fig. 2. TOCSY NMR spectra of surface marine DOM (FMAX) with **(A)**, **(B)** sensitivity enhanced apodization (exponential multiplication: EM = 7.5 Hz in F2; $\pi/2.5$ shifted sine bell in F1) to emphasize **(A)** faint and extended NMR signatures of unsaturated chemical environments in marine DOM (cf. Fig. 13); **(B)** here, the aliphatic section is characterized by extensive overlap of abundant TOCSY cross peaks with limited overall resolution. **(C)**, **(D)** resolution enhanced apodization (Gaussian multiplication: EM: −0.4 Hz; GB: 0.6 Hz in F2; $\pi/6$ shifted sine bell in F1) to emphasize depiction of molecular complexity in marine DOM. **(C)** cross peaks of protons attached to sp^2-hybridized carbon with resolved signatures of relatively abundant molecules (olefins and aromatics); **(D)** cross peaks of protons attached to sp^3-hybridized carbon (commonly $\underline{H}$CC and $\underline{H}$CO chemically environments) with resolved cross peak patterns for, e.g. alkylated/desoxy (dotted box a) and standard carbohydrates (dotted box b).

Title Page

Abstract | Introduction

Conclusions | References

Tables | Figures

◀◀ | ▶▶

◀ | ▶
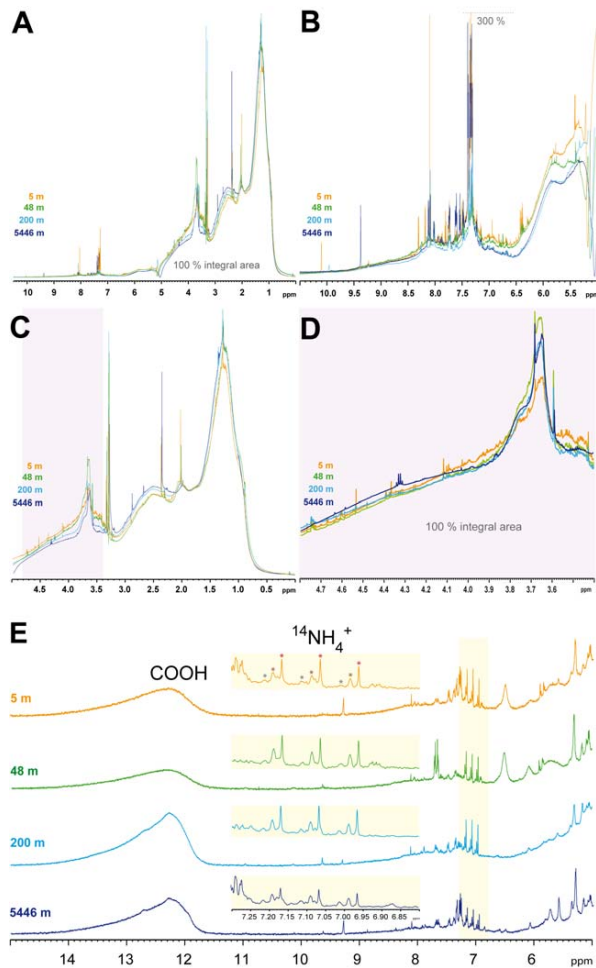
Back | Close

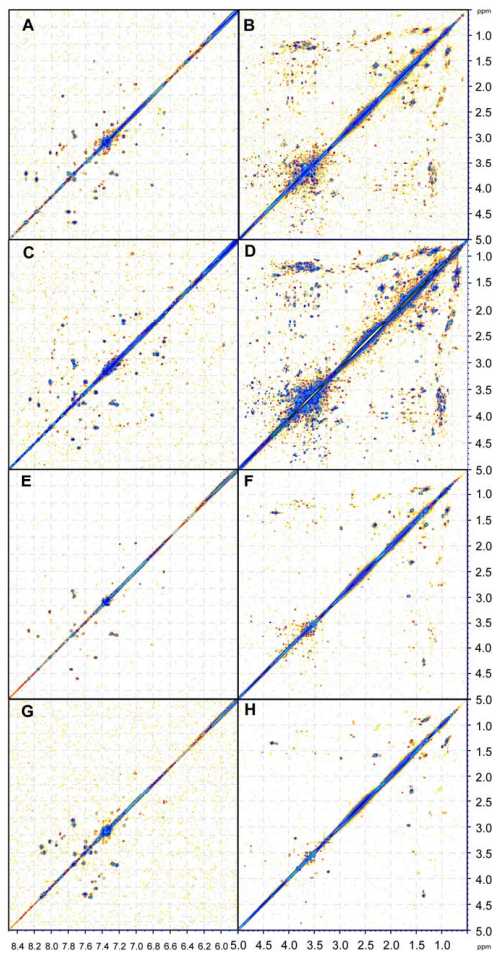Full Screen / Esc

Printer-friendly Version

Interactive Discussion

Fig. 3. (Caption on next page.)

Fig. 3. **(A)** ^{1}H NMR spectra of marine DOM obtained by solid phase extraction (PPL) at different depths according to color: orange: 5 m (FISH, near surface photic zone); green: 48 m (FMAX, fluorescence maximum); blue: 200 m (upper mesopelagic zone); dark blue: 5446 m (30 m above ground). In panels **(A)**–**(C)**, the respective spectral intensities were scaled to 100 % total integral within the entire region of chemical shift ($\delta_H \sim 0 \ldots 10.5$ ppm; with residual water and methanol excluded). **(A)** Entire spectral range, $\delta_H \sim 0 \ldots 10.5$ ppm; **(B)** unsaturated protons, bound to sp^2-hybridized carbon $\delta_H \sim 5 \ldots 10.5$ ppm and anomeric protons ($\delta_H < 5.5$ ppm); truncated at 33 % maximum intensity; cf. Supporting Online Fig. 2; **(C)** protons bound to sp^3-hybridized carbon, $\delta_H \sim 0 \ldots 5$ ppm; **(D)** section of $\underline{H}$C-O protons, normalized to 100 % integral within the chemical shift indicated ($\delta_H \sim 3.4 \ldots 4.8$ ppm); note the different relative NMR resonance amplitudes compared with panel **(C)** which is normalized to the entire range of chemical shift ($\delta_H \sim 0 \ldots 10.5$ ppm). **(E)** ^{1}H NMR spectra of marine DOM in dry DMSO-d$_6$, downfield section $\delta_H > 5$ ppm; acquired at $B_0 = 11.7$ T, showing both exchangeable and non-exchangeable protons; aside from the large carboxylic acid NMR resonance near $\delta_H \sim 12.3$ ppm ($\delta_H \sim 11.6 \ldots 14.7$ ppm), a minimum of three different ammonium (^{14}NH$_4^+$) chemical environments were observed near $\delta_H \sim 7.07$ ppm with an ostentatious coupling between ^{14}N and ^{1}H (^{1}J$_{NH} = 51.2$ Hz; 1:1:1 triplett, because of nuclear spin for ^{14}N = 1, denoted with colored asterisks).
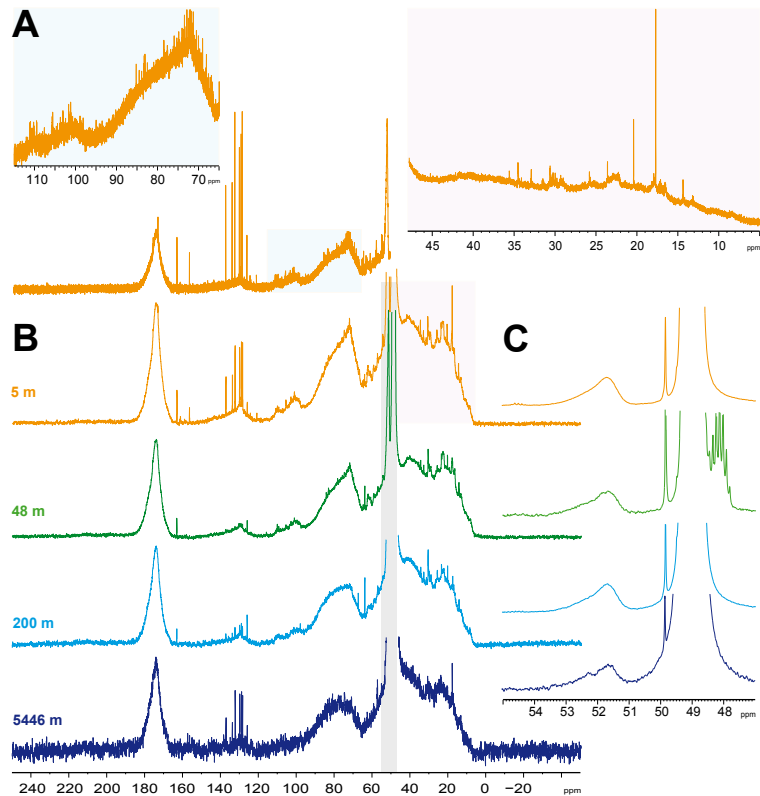
Fig. 4. ^{13}C NMR spectra of marine DOM obtained by solid phase extraction (PPL) at different depths indicated by color: 5 m (FISH, near surface photic zone); 48 m (FMAX, fluorescence maximum); 200 m (upper mesopelagic zone); 5446 m (30 m above ground); panel **(A)** apodization, exponential multiplication with LB = 1 Hz, showing resolved NMR resonances from abundant molecules; panel **(B)** apodization, exponential multiplication with LB = 12.5 Hz, fair compromise between decent resolution and S/N ratio; panel **(C)** apodization, exponential multiplication with LB = 5 Hz (methoxy NMR resonances).

Title Page

Abstract | Introduction

Conclusions | References

Tables | Figures

|◄ | ►|

◄ | ►

Back | Close

Full Screen / Esc

Printer-friendly Version

Interactive Discussion
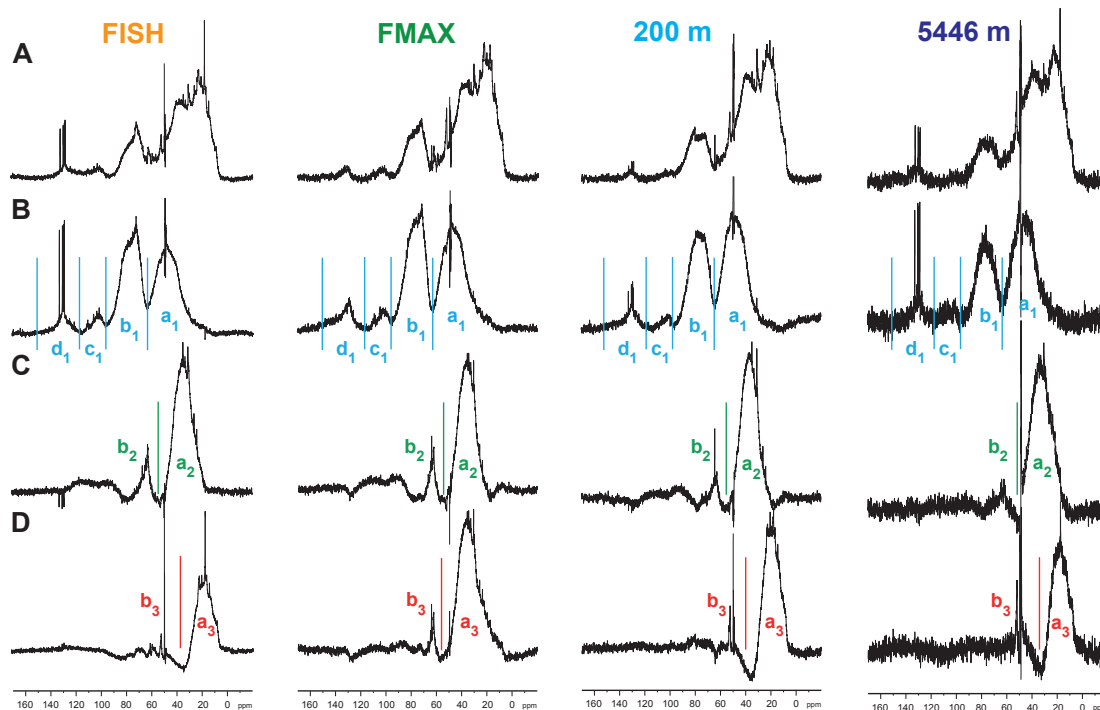
Fig. 5. ^{13}C NMR spectra for marine DOM obtained by solid phase extraction (PPL) at different depths (from left to right); **(A)** superimposed protonated carbon NMR resonances (CH$_{123}$; DEPT-45 ^{13}C NMR spectra), multiplicity-edited ^{13}C NMR spectra are **(B)** CH; methine, with indices a_1-d_1 denoting following chemical environments: **HC**$_{ar}$-C/O-**HC**-O/**HC**-O/**HC**-C), **(C)** CH$_2$; methylene, with indices a_2 and b_2 denoting following chemical environments: **H$_2$C-O/H$_2$C-C**, and **(D)** CH$_3$; methyl, with indices a_3 and b_3 denoting following chemical environments: **H$_3$C-O/H$_3$C-C**. The respective section integrals are provided in Table 4.

Title Page

Abstract | Introduction

Conclusions | References

Tables | Figures

|◄ | ►|

◄ | ►

Back | Close

Full Screen / Esc

Printer-friendly Version

Interactive Discussion

Fig. 6. (Caption on next page.)

Fig. 6. ^{1}H, ^{1}H JRES NMR spectra of **(A)**, **(C)**, **(E)**, **(G)** downfield ($\delta_H = 5.8 \ldots 8.5$ ppm; aromatic and olefinic C-$C_{sp2}\underline{H}$-$C_{sp2}\underline{H}$-C cross peaks) and **(B)**, **(D)**, **(F)**, **(H)** upfield ^{1}H NMR chemical shift region ($\delta_H = 0.5 \ldots 5.0$ ppm; aliphatic C-$\underline{HC}$-$\underline{HC}$-X (X: C, N, O) cross peaks; **(A)**, **(B)**: 5 m (FISH, near surface photic zone); **(C)**, **(D)**: 48 m (FMAX, fluorescence maximum); **(E)**, **(F)**: 200 m (upper mesopelagic zone); **(G)**, **(H)**: 5446 m (30 m above ground). **(a)** α,β-unsaturated carbonyl compounds with $^nJ_{HH} > 7$ Hz; **(b)** olefinic protons with small (remote) couplings $^nJ_{HH} \leq 3$ Hz indicative of natural products; **(c)** isolated olefinic protons with small couplings $^nJ_{HH} < 1$ Hz, possibly at quaternary bridgehead carbon; **(d)** methoxy groups [which only exhibit long range couplings $^nJ_{HH}$ (n = 4 for methyl ethers and n = 5 for methyl esters, respectively); cf. Fig. 9C] coupling constants; **(e)** methyl protons: acetate derivatives ($\delta_H > 1.9$ ppm) and aliphatic methyl ($\delta_H < 1.6$ ppm); panel **(f)**: methyl bound to methine (doublet, $^3J_{HH} \sim 7$ Hz) and methylene (triplett, $^3J_{HH} \sim 7$ Hz).

Fig. 7. (Caption on next page.)

Fig. 7. ^{1}H,^{1}H COSY NMR spectra of **(A)**, **(C)**, **(E)**, **(G)** downfield ($\delta_H = 5.8\ldots 8.5$ ppm; aromatic and olefinic C-C$_{sp^2}$$\underline{\text{H}}$-C$_{sp^2}$$\underline{\text{H}}$-C cross peaks) and **(B)**, **(D)**, **(F)**, **(H)** upfield ^{1}H NMR chemical shift region ($\delta_H = 0.5\ldots 5.0$ ppm; aliphatic C-$\underline{\text{HC}}$-$\underline{\text{HC}}$-X (X: C, N, O) cross peaks; **(A)**, **(B)**: 5 m (FISH, near surface photic zone); **(C)**, **(D)**: 48 m (FMAX, fluorescence maximum); **(E)**, **(F)**: 200 m (upper mesopelagic zone); **(G)**, **(H)**: 5446 m (30 m above ground).
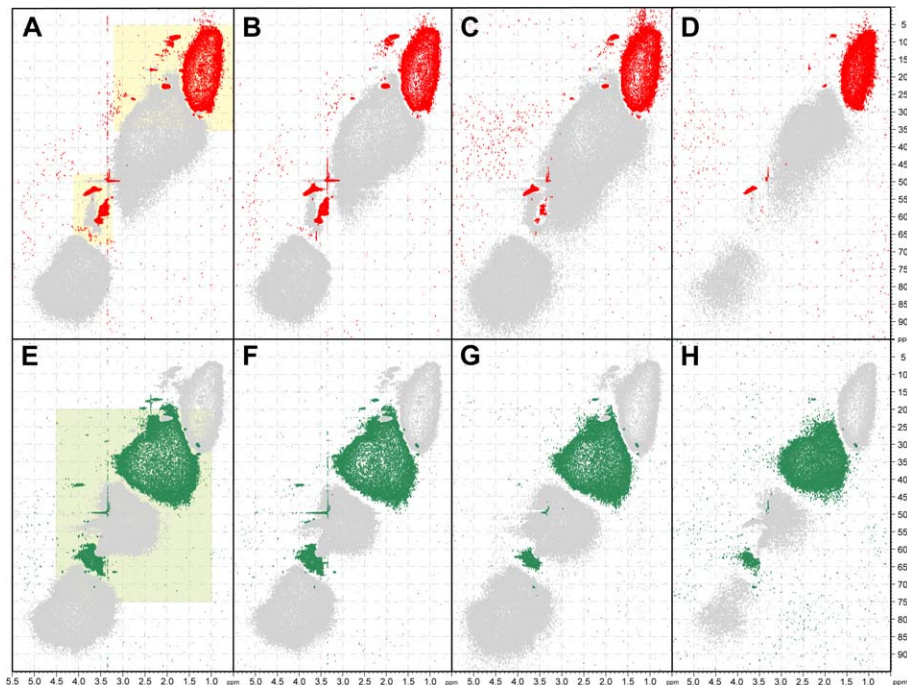
Fig. 8. DEPT HSQC NMR spectra of four marine DOM, aliphatic (**HC**C and **HC**X, with X = O, N, S) section with methyl (red) and methylene (green) cross peaks indicated; boxes denote ranges for cross peaks assignments given in Fig. 9, yellow: CH_3-selective and green: CH_2-selective DEPT HSQC NMR spectra; top panel: CH_3-selective DEPT HSQC NMR spectra (CH_3 red, CH and CH_2: gray); lower panel: CH_2-selective DEPT HSQC NMR spectra (CH_2 green, CH_3 and CH: gray). **(A)**, **(E)**: 5 m (FISH; near surface photic zone); **(B)**, **(F)**: 48 m (FMAX, fluorescence maximum); **(C)**, **(G)**: 200 m (upper mesopelagic zone); **(D)**, **(H)**: 5446 m (30 m above ground).
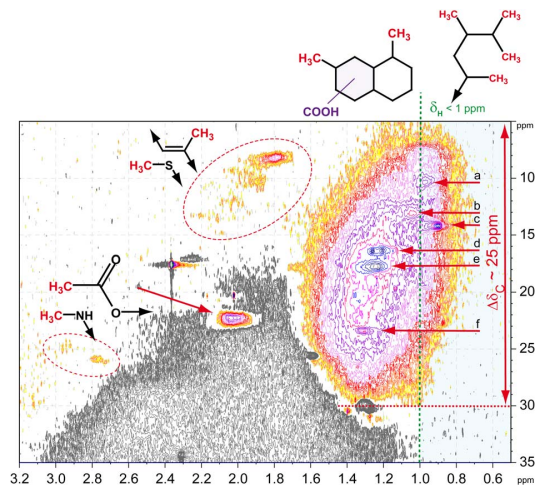
Fig. 9A. DEPT HSQC NMR spectra of surface marine DOM FISH. Section of $\underline{H}_3\underline{C}$-C cross peaks with fundamental substructures indicated; blue: the proton chemical shift range ($\delta_H < 1$ ppm) corresponding to classical methyl terminating purely aliphatic units (like, e.g. peptide side chains) contributed only <15 % of total DEPT HSQC methyl cross peak integral (in all four DOM). The sizable expansion of carbon chemical shift for $\underline{H}_3\underline{C}$-C units ($\Delta\delta_C \sim 5\ldots30$ ppm) indicated near maximum diversity of remote aliphatic substitution, i.e. maximum diversity of aliphatic branching occurred in all four marine DOM (cf. Fig. 8). The bulk of aliphatic methyl experienced downfield shift from the chemical shift anisotropy of nearby carbonyl derivatives COX, most likely carboxylic groups, causing downfield proton chemical shifts up to $\delta_H \sim 1.6$ ppm. Alicyclic aliphatic geometry (Cho et al., 2011) favours large abundance of proximate COX with respect to given counts of methyl groups, supporting the occurrence of CRAM (carboxyl-rich alicyclic molecules) as abundant contributors to marine DOM (Hertkorn et al., 2006; Lam et al., 2007; Leenheer et al., 2003). The six recognizable intensity maxima of aliphatic methyl (denoted: a–f) likely reflected superposition of remotely substituted common geometries of aliphatic branching. Methyl groups attached to olefins were common; minor suites of S-CH$_3$ groups might also have occurred in this cross peak section. Acetate derivatives and a few minor N-CH$_3$ groups complemented the major $\underline{H}_3\underline{C}$-C chemical environments shown.
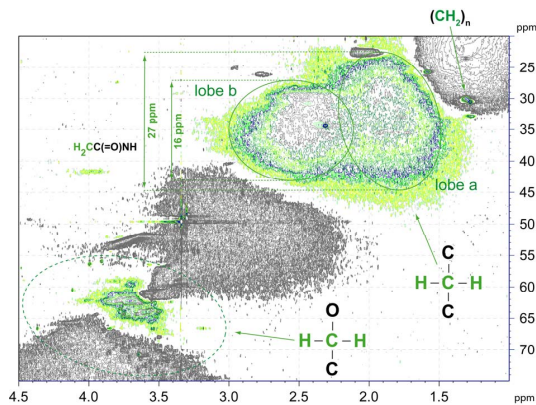
Fig. 9B. DEPT HSQC NMR spectra of surface marine DOM FISH. Section of $\underline{H_2C}$-Z [Z = C, O, (N, S)] cross peaks. Polymethylene $(CH_2)_n$ experiences the least number of aliphatic neighbours and occupies a low intensity cross peak (<1 % of methylene cross peak integral) in a confined area at high field. Carbon bound methylene decompose into two major lobes; the right lobe a ($\delta_H \sim 1.5\ldots2.2$ ppm) occupied a sizable carbon chemical shift range ($\Delta\delta_C$) of 27 ppm, whereas the lower field lobe b ($\delta_H \sim 2.2\ldots3.0$ ppm) occupied a smaller carbon chemical shift range ($\Delta\delta_C$) of 16 ppm. These two units differ in the position of COX derivatives with respect to the observed $\underline{H_2C}$-Z unit, which is directly adjacent for lobe b (i.e. CH_2-COX) and two or more bounds away for lobe a. COX at positions one (α-position) and two (β-position) bonds away from methylene carbon will displace aliphatics which otherwise would impose sizable carbon downfield shifts in the range of ($\Delta\delta_C \sim 9$ ppm); in addition, proximate COX derivatives will cause downfield proton chemical shift because of chemical shift anisotropy of the carbonyl group (lobe b). COX at positions three (γ-position) bonds away from methylene carbon will cause lesser chemical shift anisotropy in proton NMR and obviate a shielding increment for γ-aliphatic substitution ($\Delta\delta_C$: -0.8 ppm), leaving δ_C and δ_H nearly unaltered from standard aliphatic (branched) substitution (lobe a). Several recognizable intensity maxima of aliphatic methylene C-$\underline{CH_2}$-C likely reflected superposition of remotely substituted common geometries of aliphatic branching. Oxomethylene ($\underline{H_2C}$-O) chemical environments in marine DOM commonly represent carbohydrate side chains of considerable diversity alongside with other minor oxomethylene cross peaks.

Title Page

Abstract | Introduction

Conclusions | References

Tables | Figures

◀ | ▶

◀ | ▶

Back | Close

Full Screen / Esc

Printer-friendly Version

Interactive Discussion

Full Screen / Esc
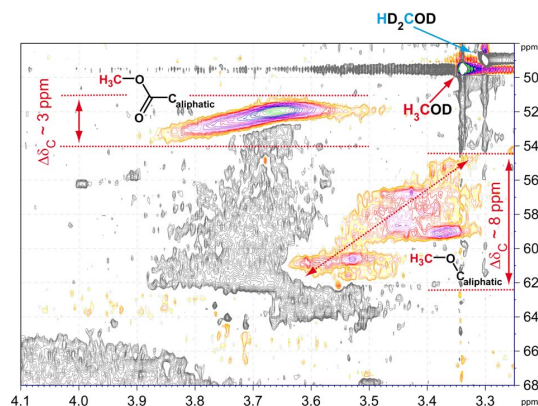
Fig. 9C. DEPT HSQC NMR spectra of surface marine DOM FISH. Section of $\underline{H}_3\underline{C}$-O cross peaks with two major substructures indicated: methyl esters and methyl ethers, respectively. Methyl ethers were more abundant than in freshwater and soil DOM and occupied a sizable range of carbon chemical shifts ($\delta_H \sim 55\ldots62$ ppm), given the minimum distance of four bonds from the methyl proton to the first optional variance in substitution ($^4J_{ZH}$ for $\underline{H}_3$C-O-C-$\underline{Z}$ [Z = C, O, (N, S)]; likewise, the sizable spread of proton methoxyl chemical shift ($\delta_H \sim 3.35\ldots3.65$ ppm) indicated substantial chemical diversity of methyl ethers found in marine DOM. The rather limited bandwidth of carbon chemical shifts in methyl esters ($\Delta\delta_C \sim 3$ ppm) reflects the mandatory minimum distance of five bonds from the methyl proton to the first optional variance in substitution ($^5J_{ZH}$ for $\underline{H}_3$C-O-C(=O)-C-$\underline{Z}$ [Z = C, O, N, S]; the sizable spread of proton chemical shifts ($\delta_H \sim 3.5\ldots3.85$ ppm) nevertheless indicated substantial chemical diversity of methyl esters found in marine DOM. Judging from the one-dimensional ^{1}H NMR spectra (Fig. 3D), the relative disappearance of the DEPT HSQC methyl ether cross peak from surface to deep marine DOM (Fig. 8) likely reflected real disappearance of methyl ethers from surface to deep DOM rather than NMR relaxation imposed bleaching.
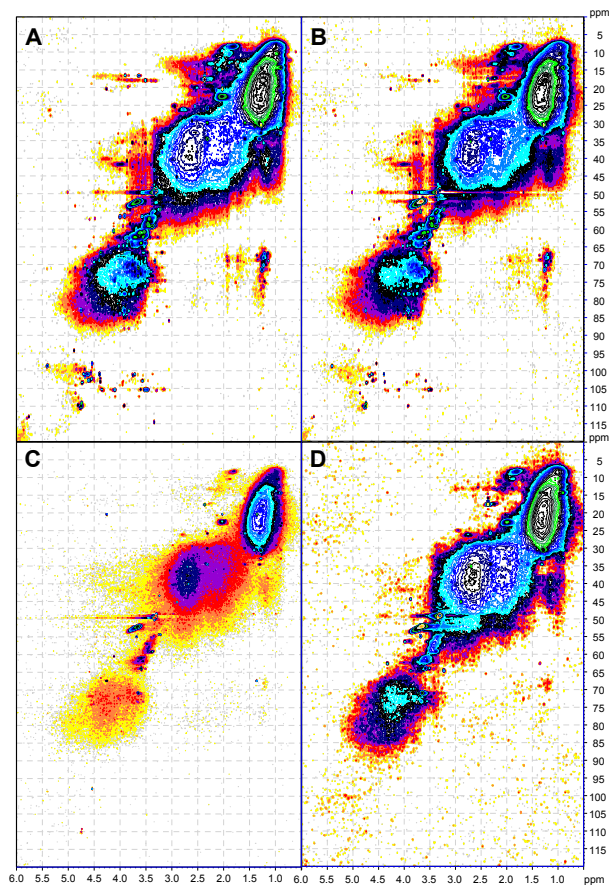
Fig. 10. HSQC TOCSY NMR spectra of four marine DOM, aliphatic section of sp³-hybridized carbon **(A)** 5 m (FISH, near surface photic zone); **(B)** 48 m (FMAX, fluorescence maximum); **(C)** 200 m (upper mesopelagic zone); **(D)** 5446 m (30 m above ground). For NMR acquisition parameters, see Supporting Online Table 1.
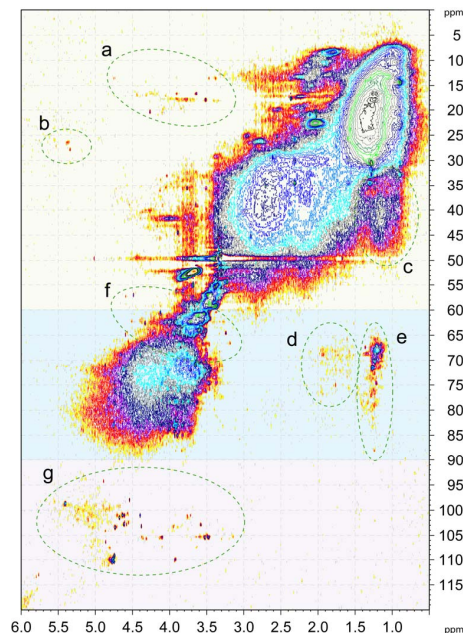
Fig. 10e. HSQC TOCSY NMR spectrum of surface marine DOM sample FMAX. Coarse substructures, connected by $^{n}J_{HH}$ (n = 2–5) are given according to color, green: $\underline{H}C(C)\underline{C}H$ (δ_C: 0...60 ppm), blue: $\underline{H}C(C)\underline{C}O$ (δ_C: 60...90 ppm), and purple: $\underline{H}C(C)H\underline{C}O_2$ (δ_C: 90...110 ppm). Section a: $\underline{H}C(C)\underline{H}CO$ substructures, like alkylated carbohydrates (Panagiotopoulos et al., 2007); section b: $\underline{H}C(C)H\underline{C}(=O)O$ substructures, like esters and multiply oxygenated aliphatics; section c: $\underline{H}C(C)H\underline{C}C$ substructures, like functionalized and strongly branched aliphatics; section d: $C\underline{H}C(C)H\underline{C}O$ substructures, aliphatics connected to oxygenated carbon, like alkylated carbohydrates and ethers; section e: $\underline{H}_3C(C)H\underline{C}O$ substructures, methyl connected to oxygenated carbon, like methylated carbohydrates and ethers; section f: $\underline{H}_3CO(C)H\underline{C}O$ substructures, like methoxyl bound to oxygenated carbon; section g: $CH\underline{C}O(\overline{C})\underline{H}CO_2$ substructures, connecting anomerics in carbohydrates with adjacent rings (significant confirmation tool for carbohydrates).

Title Page

Abstract | Introduction

Conclusions | References

Tables | Figures

◄ | ►

◄ | ►

Back | Close

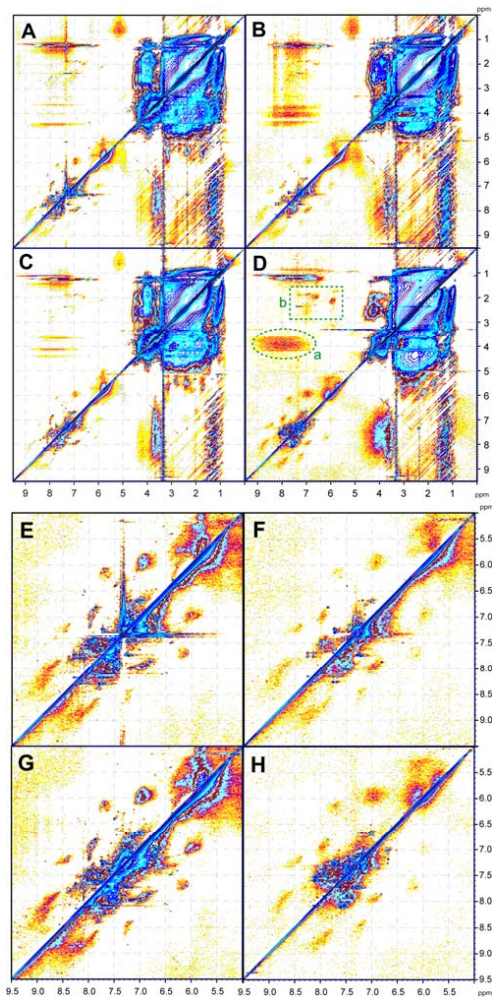Full Screen / Esc

Printer-friendly Version

Interactive Discussion
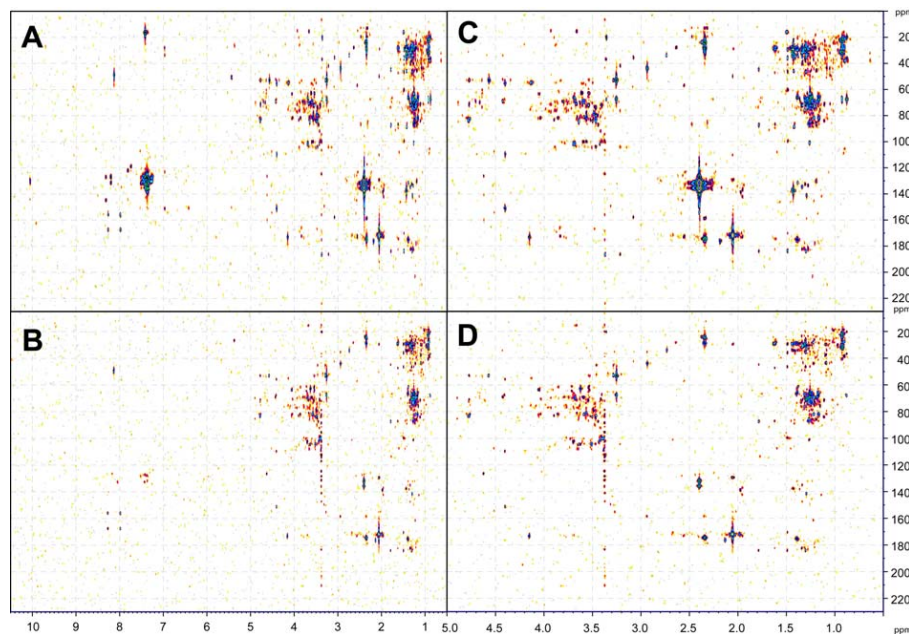
Fig. 11. ^{1}H, ^{13}C HMBC spectra of **(A)**, **(C)** surface DOM FISH (near surface photic zone) and **(B)**, **(D)** surface DOM FMAX (fluorescence maximum); aliphatic section.

Full Screen / Esc
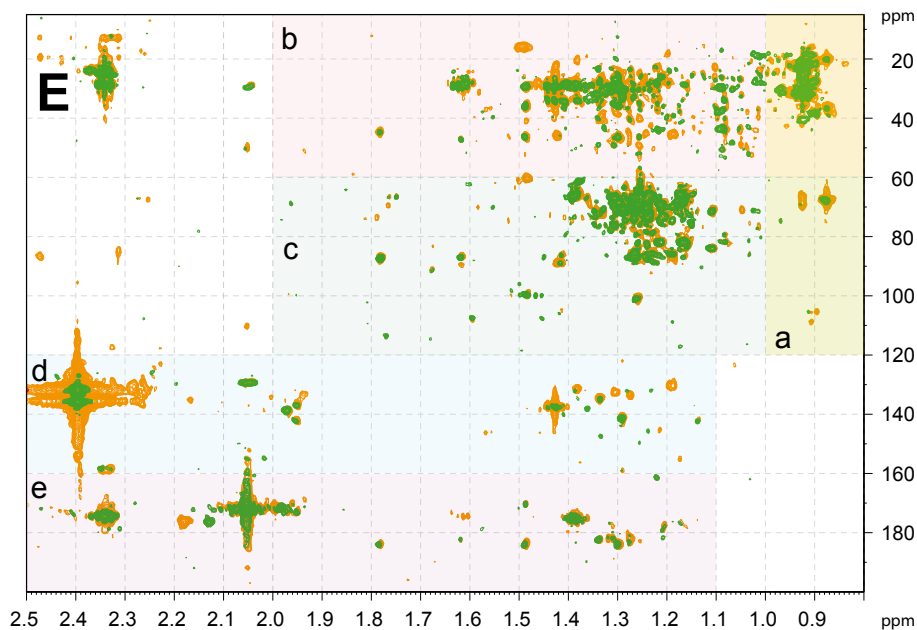
Fig. 11E. (E) superposition of surface FISH (orange) and FMAX (green) HMBC cross peaks with substructure regimes indicated: panel **(A)** HMBC cross peaks $^{2,3}J_{CH}$ connecting methyl with various groups: $\underline{H}_3C\text{-}(C)\underline{C}C$ ($\delta_C < 60$ ppm), $\underline{H}_3C\text{-}(C)\underline{C}O$ ($\delta_C < 60\ldots100$ ppm), and $\underline{H}_3C\text{-}(C)\underline{C}O_2$ ($\delta_C < 60\ldots100$ ppm); **(B)** intra aliphatic HMBC cross peaks $\underline{H}C(C)\underline{C}$ ($^{2,3}J_{CH}$); **(C)** intra aliphatic HMBC cross peaks $\underline{H}C(C)\underline{C}O$ ($^{2,3}J_{CH}$); **(D)** HMBC cross peak connecting aliphatic protons with sp^2-hybridized carbon (olefin or aromatics) $\underline{H}C_{al}(C)\underline{C}_{sp^2}(^{2,3}J_{CH})$; **(E)** HMBC cross peak connecting aliphatic protons with carbonyl carbon (olefin or aromatics) $\underline{H}C_{al}(C)\underline{C}(=O)X(^{2,3}J_{CH})$.

Discussion Paper | Discussion Paper | Discussion Paper | Discussion Paper | Discussion Paper

Title Page

Abstract | Introduction

Conclusions | References

Tables | Figures

|◄ | ►|

◄ | ►

Back | Close

Full Screen / Esc

Printer-friendly Version

Interactive Discussion
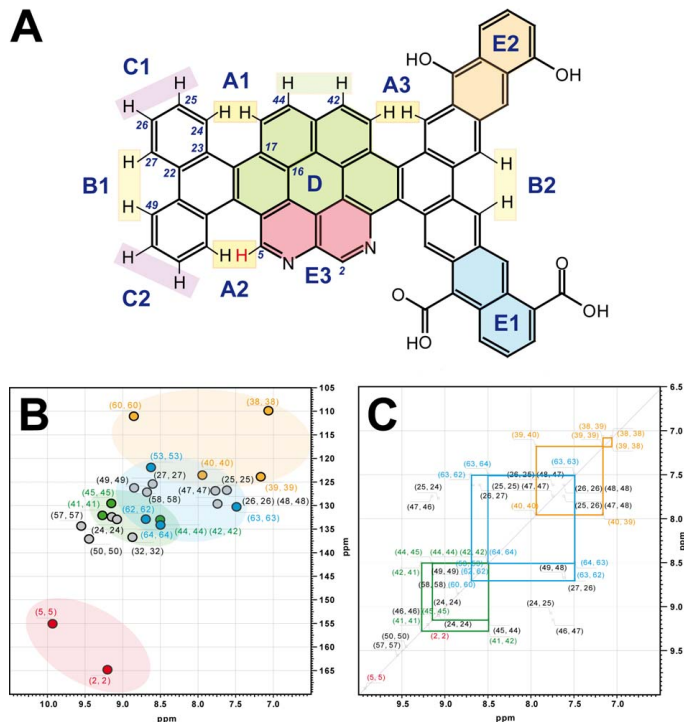
Fig. 12. Conceptual model of polycyclic aromatics to elucidate prospective NMR properties of marine thermogenic carbon (TMOC; cf. text). **(A)** molecular formula of PAH model $C_{65}H_{34}N_2O_6$ (IUPAC mass: 938.975 Da) with specific chemical environments provided (full numbering scheme cf. Supporting Online Fig. 5, ^{1}H and ^{13}C NMR chemical shifts: Supporting Online Table 2): narrow polycyclic hydrocarbon (PAH) fjord regions: A1, A2, A3; more relaxed open PAH bay regions: B1 and B2; unconstrained PAH: C1 and C2; condensed PAH: D; specific substitutions patterns as follows: electron withdrawing substituents: E1; electron-donating substitution: E2; N-heterocycles: E3. **(B)** computed HSQC and **(C)** COSY (TOCSY) NMR spectra of PAH model $C_{65}H_{34}N_2O_6$ with specific positions highlighted (cf. text).

Fig. 13. (Caption on next page.)

Full Screen / Esc

Fig. 13. TOCSY NMR cross peaks of four marine DOM [**(A)**, **(E)** 5 m (FISH, near surface photic zone); **(B)**, **(F)** 48 m (FMAX, fluorescence maximum); **(C)**, **(G)** 200 m (upper mesopelagic zone); **(D)**, **(H)**: 5446 m (30 m above ground)] with sensitivity enhanced apodization to emphasize less abundant sp^2-hybridized carbon environments in marine DOM. **(A)**–**(D)** full spectrum δ_H = 0...9.5 ppm; **(E)**–**(H)** section of unsaturated (olefinic and aromatic) protons δ_H = 5...9.5 ppm; **(D)** dotted box a: TOCSY cross peaks connecting peptides $\underline{H}$N-C$\underline{H}\alpha$; dotted box b: TOCSY cross peaks connecting olefins and methyl, C=$\underline{H}$C-C$\underline{H}_3$.

Full Screen / Esc
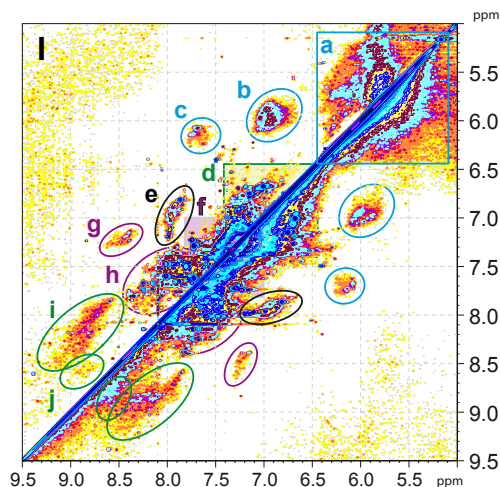
Fig. 13I. (I) Unsaturated (olefinic and aromatic) protons in surface sample FMAX with substructures denoted as follows: section a: intra olefinic cross peaks $\underline{H}C_{olefin}=C_{olefin}\underline{H}$, like in linear terpenoids; section b: α,β-unsaturated double bonds: $\underline{H}C_{olefin}=C_{olefin}\underline{H}$-(C=O)-X; section c: polarized α,β-unsaturated double bonds: $\underline{H}C_{olefin}=C_{olefin}\underline{H}$-(C=O)-X; section d: aromatics $\underline{H}C_{aromatic}$-$C_{aromatic}\underline{H}$ with ortho or/and para oxygenated substituents (classic aromatic substitution of natural organic matter); section e: strongly polarized α,β-unsaturated double bonds, also in oxygen-derived heterocycles: $\underline{H}C_{olefin}$-$C_{olefin}\underline{H}$-(C=O, O)-X; section f: condensed and strongly electron withdrawing aromatics $\underline{H}C_{aromatic}$-$C_{aromatic}\underline{H}$ (multiply carboxylated, N-heterocycles); section g: polycyclic aromatics, open fjord region (cf. Fig. 13A sections B1, B2), N-heterocycles; section h: polycyclic aromatics, fjord region in polycyclic aromatics, more extended polycyclic aromatics, N-heterocycles; section i: congested fjord region in polycyclic aromatics (cf. Fig. 13A sections A1, A2, A3).

Fig. 14. (Caption on next page.)

Title Page

Abstract | Introduction

Conclusions | References

Tables | Figures

◄ | ►

Back | Close

Full Screen / Esc

Printer-friendly Version

Interactive Discussion

Fig. 14. ^{1}H, ^{13}C HSQC NMR cross peaks of four marine DOM with **(A)** four major chemical environments indicated [**(A)**, **(E)** 5 m (FISH, near surface photic zone); **(B)**, **(F)** 48 m (FMAX, fluorescence maximum); **(C)**, **(G)** 200 m (upper mesopelagic zone); **(D)**, **(H)** 5446 m (30 m above ground)] with sensitivity enhanced apodization to emphasize less abundant sp^2-hybridized carbon environments in marine DOM. **(A)**–**(D)** full spectra $\delta_H = 0\ldots10$ ppm; **(E)**–**(H)** section of unsaturated (olefinic and aromatic) protons $\delta_H = 5\ldots10.5$ ppm.
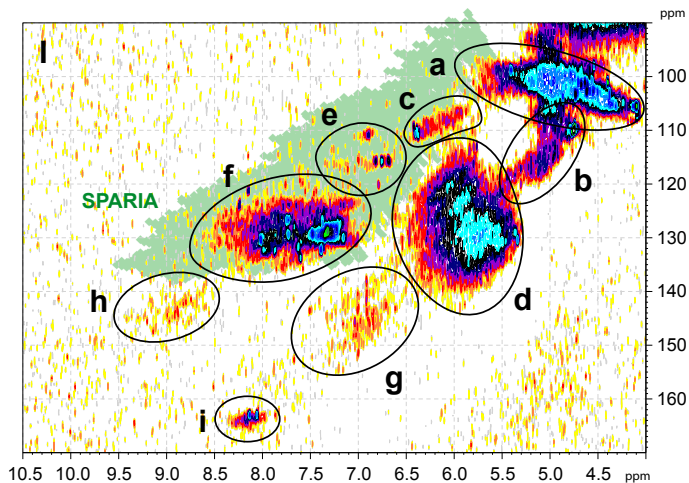
Fig. 14I. (I) Section of unsaturated (olefinic and aromatic) CH pairs in surface sample FMAX (fluorescence maximum) with substructures denoted as follows: section a: anomeric CH in carbohydrates (sp³-hybridized); section b: isolated olefins; section c: multiply oxygenated aromatics (oxygen heterocycles), olefins; section d: C-conjugated olefins, certain five membered N-, O- and S-heterocycles ($\delta_H < 6.5$ ppm); section e: phenols, classical oxygenated NOM aromatics ; section f: classical NOM aromatics with substantial fraction of carbonyl derivatives (likely COOH); at $\delta_H > 8$ ppm: multiply carboxylated aromatics, classical PAH and six-membered nitrogen heterocycles; sterically uncongested polycyclic aromatic hydrocarbons; section g: α,β-unsaturated double bonds for $\delta_C > 140$ ppm, including double bonds adjacent to aromatics: C-$\underline{\text{HC}}_{\text{olefin}}$=$\underline{\text{C}}_{\text{olefin}}\underline{\text{H}}$-(C=O, C$_{ar}$)-X; section h: nitrogen heterocycles, heteroatom substituted polycyclic aromatics; section i: specific nitrogen heterocycles, very likely with more than one nitrogen. The green area highlights the HSQC cross peak region accessible to single benzene rings substituted by common electron withdrawing, neutral and electron-donating common substituents of natural organic matter; SPARIA: Substitution Patterns in Aromatic Rings by Increment Analysis (Perdue et al., 2007).
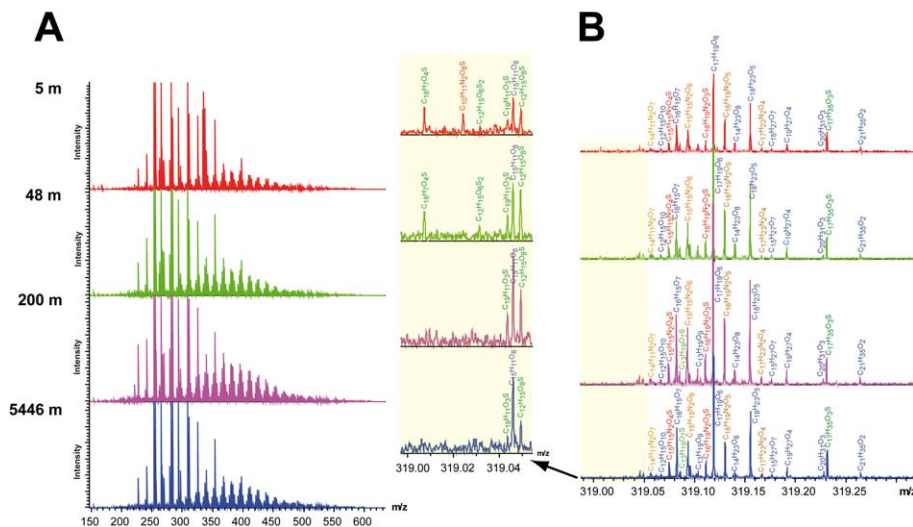
Title Page

Abstract | Introduction

Conclusions | References

Tables | Figures

|◄ | ►|

◄ | ►

Back | Close

Full Screen / Esc

Printer-friendly Version

Interactive Discussion

Fig. 15. Negative electrospray 12T FTICR mass spectra of marine DOM samples; from top to bottom: 5 m (FISH, near surface photic zone); 48 m (FMAX, fluorescence maximum); 200 m (upper mesopelagic zone); 5446 m (30 m above ground). **(A)** FTICR mass spectra from 150–700 Da; **(B)** expansion of nominal mass 319 for negative ions MH^- with molecular formulas provided on the basis of their mass accuracy and mass resolution (cf. text). Insert panel **(B)** expansion of the mass segment 319–319.05 Da ($\Delta m = 0.05$ Da) with enhanced relative intensity, indicating mostly CHOS molecules which discriminate between top and bottom marine DOM (Fig. 16).
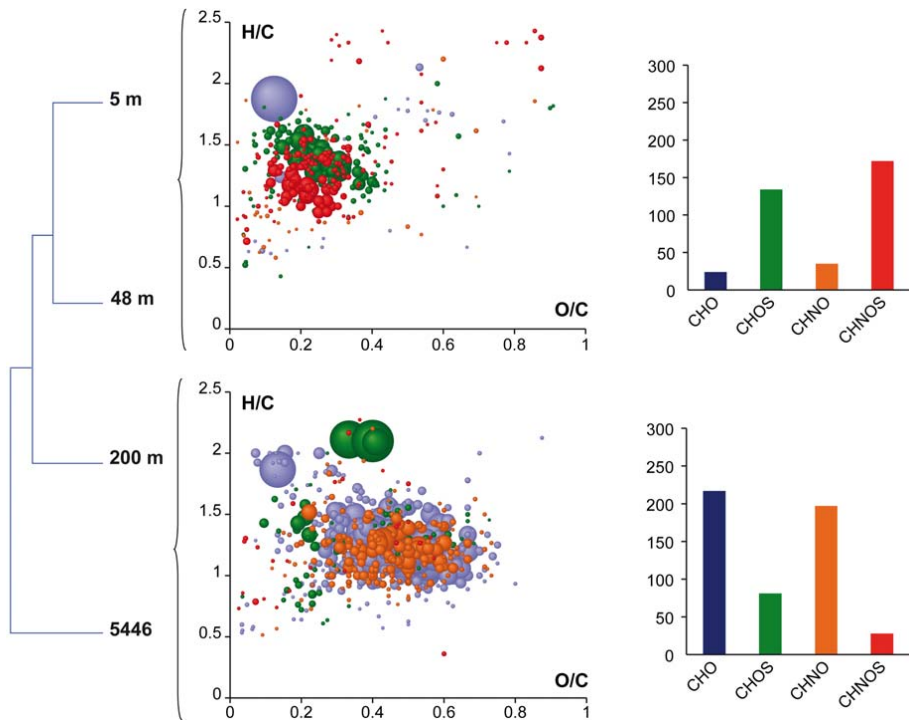
Fig. 16. Left panel: Euclidean clustering diagram based on the similarity values between the merged FTICR mass spectra of marine DOM near surface (5, 48 m) and at depth (200, 5446 m); circular areas indicate relative mass peak intensity. Top: van Krevelen diagrams of the unique compounds found in 5/48 m depths versus 200/5446 m depths; Down: van Krevelen diagrams of the unique compounds found in 200/5446 m depths versus 5/48 m depths. Right panel: histograms represent counts of respective unique CHO, CHOS, CHNO and CHNOS containing molecules.

Title Page

Abstract | Introduction

Conclusions | References

Tables | Figures

◄ | ►I

◄ | ►

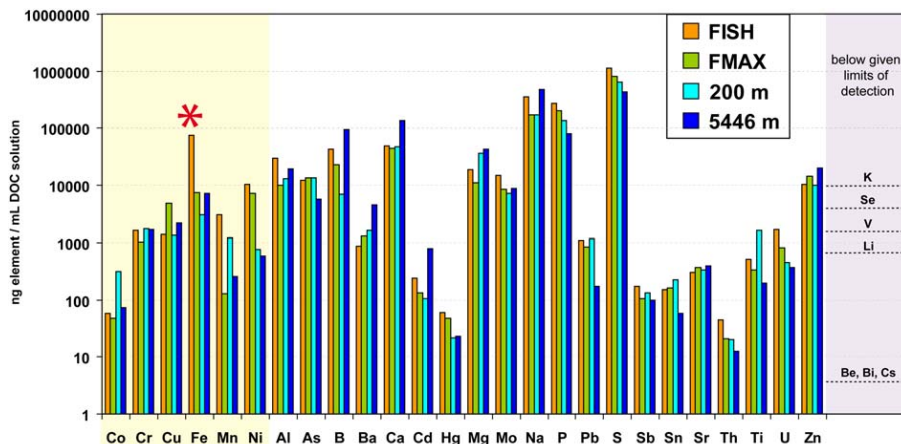Back | Close

Full Screen / Esc

Fig. 17. Content of metals/elements in methanolic DOM solutions to assess metal contribution to NMR relaxation (note logarithmic display of concentration), yellow: significant metals capable of forming paramagnetic coordination compounds with marine DOM, with iron (Fe) in surface DOM FISH as the most abundant (asterisk; cf. text); purple background: elements Be, Bi, Cs, K, Li, Se and V were found below detection limits indicated (cf. Supporting Online Table 3).